

1 Dissolved iron in the North Atlantic Ocean and Labrador Sea along 2 the GEOVIDE section (GEOTRACES section GA01)

3 Manon Tonnard^{1,2,3}, H el ene Planquette¹, Andrew R. Bowie^{2,3}, Pier van der Merwe², Morgane Gallinari¹,
4 Floriane Desprez de G esincourt¹, Yoan Germain⁴, Arthur Gourain⁵, Marion Benetti^{6,7}, Gilles Reverdin⁷,
5 Paul Tr eguer¹, Julia Boutorh¹, Marie Cheize¹, Fran ois Lacan⁸, Jan-Lukas Menzel Barraqueta^{9,10},
6 Leonardo Pereira-Contreira¹¹, Rachel Shelley^{1,12,13}, Pascale Lherminier¹⁴, G eraldine Sarthou¹

7 ¹Laboratoire des sciences de l'Environnement MARin – CNRS UMR 6539 – Institut Universitaire Europ een de la Mer,
8 Universit e de Bretagne Occidentale, Plouzan e, 29280, France

9 ²Antarctic Climate and Ecosystems – Cooperative Research Centre, University of Tasmania, Hobart, TAS 7001, Australia

10 ³Institute for Marine and Antarctic Studies, University of Tasmania, Hobart, TAS 7001, Australia

11 ⁴Laboratoire Cycles G eochimiques et ressources – Ifremer, Plouzan e, 29280, France

12 ⁵Ocean Sciences Department, School of Environmental Sciences, University of Liverpool, L69 3GP, UK

13 ⁶Institute of Earth Sciences, University of Iceland, Reykjavik, Iceland

14 ⁷LOCEAN, Sorbonne Universit es, UPMC/CNRS/IRD/MNHN, Paris, France

15 ⁸LEGOS, Universit e de Toulouse - CNRS/IRD/CNES/UPS – Observatoire Midi-Pyr en es, Toulouse, France

16 ⁹GEOMAR Helmholtz-Zentrum f ur Ozeanforschung Kiel Wischhofstra e 1-3, Geb. 12 D-24148 Kiel, Germany

17 ¹⁰Department of Earth Sciences, Stellenbosch University, Stellenbosch, 7600, South Africa

18 ¹¹Funda  o Universidade Federal do Rio Grande (FURG), R. Luis Lor ea, Rio Grande –RS, 96200-350, Brazil

19 ¹²Dept. Earth, Ocean and Atmospheric Science, Florida State University, 117 N Woodward Ave, Tallahassee, Florida, 32301,
20 USA

21 ¹³School of Geography, Earth and Environmental Sciences, University of Plymouth, Drake Circus, Plymouth, PL4 8AA, UK

22 ¹⁴Ifremer, Universit e de Bretagne Occidentale (UBO), CNRS, IRD, Laboratoire d'Oc eanographie Physique et Spatiale
23 (LOPS), IUEM, F-29280, Plouzan e, France

24

25 *Correspondence to:* Manon Tonnard (Manon.Tonnard@utas.edu.au)

26

27 **Abstract.** Dissolved Fe (DFe) samples from the GEOVIDE voyage (GEOTRACES GA01, May-June 2014) in the North
28 Atlantic Ocean were analysed using a SeaFAST-picoTM coupled to an Element XR SF-ICP-MS and provided interesting
29 insights on the Fe sources in this area. Overall, DFe concentrations ranged from 0.09 ± 0.01 nmol L⁻¹ to 7.8 ± 0.5 nmol L⁻¹.
30 Elevated DFe concentrations were observed above the Iberian, Greenland and Newfoundland Margins likely due to riverine
31 inputs from the Tagus River, meteoric water inputs and sedimentary inputs. Enhanced air-sea interactions were suspected to
32 be responsible for the increase in DFe concentrations within subsurface waters of the Irminger Sea due to deep convection
33 occurring the previous winter, which provided iron-to-nitrate ratios sufficient to sustain phytoplankton growth. Increasing DFe
34 concentrations along the flow path of the Labrador Sea Water were attributed to sedimentary inputs from the Newfoundland
35 Margin. Bottom waters from the Irminger Sea displayed high DFe concentrations likely due to the dissolution of Fe-rich
36 particles in the Denmark Strait Overflow Water and the Polar Intermediate Water. Finally, the nepheloid layers located in the
37 different basins and at the Iberian Margin were found to act as either a source or a sink of DFe depending on the nature of
38 particles with organic particles likely releasing DFe and Mn-particles scavenging DFe.

1 **1 Introduction**

2 The North Atlantic Ocean is known for its pronounced spring phytoplankton blooms (Henson et al., 2009; Longhurst, 2007).
3 Phytoplankton blooms induce the capture of aqueous carbon dioxide through photosynthesis, and conversion into particulate
4 organic carbon (POC). This POC is then exported into deeper waters through the production of sinking biogenic particles and
5 ocean currents. Via these processes, and in conjunction with the physical carbon pump, the North Atlantic Ocean is the largest
6 oceanic sink of anthropogenic CO₂ (Pérez et al., 2013), despite covering only 15% of global ocean area (Humphreys et al.,
7 2016; Sabine et al., 2004) and is therefore crucial for Earth's climate.

8
9 Indeed, phytoplankton must obtain, besides light and inorganic carbon, chemical forms of essential elements, termed nutrients
10 to be able of photosynthesise. Indeed, Fe is a key element for a number of metabolic processes (e.g. Morel et al., 2008). The
11 availability of these nutrients in the upper ocean frequently limits the activity and abundance of these organisms together with
12 light conditions (Moore et al., 2013). In particular, winter nutrient reserves in surface waters set an upper limit for biomass
13 accumulation during the annual spring-to-summer bloom and will influence the duration of the bloom (Follows and
14 Dutkiewicz, 2001; Henson et al., 2009; Moore et al., 2013; 2008). Hence, nutrient depletion due to biological consumption is
15 considered as a major factor in the decline of blooms (Harrison et al., 2013).

16
17 The extensive studies conducted in the North Atlantic Ocean through the Continuous Plankton Recorder (CPR) have
18 highlighted the relationship between the strength of the westerlies and the displacement of the subarctic front (SAF), (which
19 corresponds to the North Atlantic Oscillation (NAO) index (Bersch et al., 2007)), and the phytoplankton dynamics of the
20 central North Atlantic Ocean (Barton et al., 2003). Therefore, the SAF not only delineates the subtropical gyre from the
21 subpolar gyre but also two distinct systems in which phytoplankton limitations are controlled by different factors. In the North
22 Atlantic Ocean, spring phytoplankton growth is largely light-limited within the subpolar gyre. Light levels are primarily set
23 by freeze-thaw cycles of sea ice and the high-latitude extremes in the solar cycle (Longhurst, 2007). Simultaneously, intense
24 winter mixing supplies surface waters with high concentrations of nutrients. In contrast, within the subtropical gyre, the spring
25 phytoplankton growth is less impacted by the light regime and has been shown to be N and P-co-limited (e.g. Harrison et al.,
26 2013; Moore et al., 2008). This is principally driven by Ekman downwelling with an associated export of nutrients out of the
27 euphotic zone (Oschlies, 2002). Thus, depending on the location of the SAF, phytoplankton communities from the central
28 North Atlantic Ocean will be primarily light or nutrient limited.

29
30 However, once the water column stratifies and phytoplankton are released from light limitation, seasonal high-nutrient, low
31 chlorophyll (HNLC) conditions were reported at the transition zone between the gyres, especially in the Irminger Sea and
32 Iceland Basin (Sanders et al., 2005). In these HNLC zones, trace metals are most likely limiting the biological carbon pump.
33 Among all the trace metals, Fe has been recognized as the prime limiting element of North Atlantic primary productivity (e.g.

1 Boyd et al., 2000; Martin et al., 1994; 1988; 1990). However, the phytoplankton community has been shown to become N
2 and/or Fe-(co)-limited in the Iceland Basin and the Irminger Sea (e.g. Nielsdóttir et al., 2009; Painter et al., 2014; Sanders et
3 al., 2005).

4

5 In the North Atlantic Ocean, dissolved Fe (DFe) is delivered through multiple pathways such as ice-melting (e.g. Klunder et
6 al., 2012; Tovar-Sanchez et al., 2010), atmospheric inputs (Achterberg et al., 2018; Baker et al., 2013; Shelley et al., 2015;
7 2017), coastal runoff (Rijkenberg et al., 2014), sediment inputs (Hatta et al., 2015), hydrothermal inputs (Achterberg et al.,
8 2018; Conway and John, 2014) and by water mass circulation (vertical and lateral advections, e.g. Laes et al., 2003). Dissolved
9 Fe can be regenerated through biological recycling (microbial loop, zooplankton grazing, e.g. Boyd et al., 2010; Sarthou et al.,
10 2008). Iron is removed from the dissolved phase by biological uptake, export and scavenging along the water column and
11 precipitation (itself a function of salinity, pH of seawater and ligand concentrations).

12

13 Although many studies investigated the distribution of DFe in the North Atlantic Ocean, much of this work was restricted to
14 the upper layers (< 1000 m depth) or to one basin. Therefore, uncertainties remain on the large-scale distribution of DFe in the
15 North Atlantic Ocean and more specifically within the subpolar gyre where few studies have been undertaken, and even fewer
16 in the Labrador Sea. In this biogeochemically important area, high-resolution studies are still lacking for understanding the
17 processes influencing the cycle of DFe.

18

19 The aim of this paper is to elucidate the sources and sinks of DFe, its distribution regarding water masses and assesses the
20 links with biological activity along the GEOVIDE (GEOTRACES-GA01) transect. This transect spanned several
21 biogeochemical provinces including the West European Basin, the Iceland Basin, the Irminger and the Labrador Seas (Fig. 1).
22 In doing so we hope to constrain the potential long-range transport of DFe through the Deep Western Boundary Current
23 (DWBC) via the investigation of the local processes effecting the DFe concentrations within the three main water masses that
24 constitute it: Iceland Scotland Overflow Water (ISOW), Denmark Strait Overflow Water (DSOW) and Labrador Sea Water
25 (LSW).

26 **2 Material and methods**

27 **2.1 Study area and sampling activities**

28 Samples were collected during the GEOVIDE (GEOTRACES-GA01 section, Fig. 1) oceanographic voyage from 15 May 2014
29 (Lisbon, Portugal) to 30 June 2014 (St. John's, Newfoundland, Canada) aboard N/O *Pourquoi Pas?*. The study was carried
30 out along the OVIDE line (<http://www.umr-lops.fr/Projets/Projets-actifs/OVIDE>, previously referred to as the WOCE A25
31 Greenland to Portugal section), and in the Labrador Sea (corresponding to the WOCE A01 leg 3 Greenland to Newfoundland
32 section). The OVIDE line has been sampled every two years since 2002 in the North Atlantic (e.g. Mercier et al., 2015), and

1 in the Labrador Sea (broadly corresponding to the WOCE A01 leg 3 Greenland to Newfoundland section). In total, 32 stations
2 were occupied, and samples were usually collected at 22 depths, except at shallower stations close to the Iberian, Greenland
3 and Canadian shelves (Fig. 1) where fewer samples (between 6 and 11) were collected. To avoid ship contamination of surface
4 waters, the shallowest sampling depth was 15 m at all stations. Therefore, ‘surface water samples’ refers to 15m depth.

5
6 Samples were collected using a trace metal clean polyurethane powder-coated aluminium frame rosette (hereafter referred to
7 as TMR) equipped with twenty-two 12L, externally closing, Teflon-lined, GO-FLO bottles (General Oceanics) and attached
8 to a Kevlar® line. The cleaning protocols for sampling bottles and equipment followed the guidelines of the GEOTRACES
9 Cookbook (www.geotraces.org, Cutter et al., 2017). After TMR recovery, GO-FLO bottles were transferred into a clean
10 container equipped with a class 100 laminar flow hood. Samples were either taken from the filtrate of particulate samples
11 (collected on polyethersulfone filters, 0.45 µm supor®, see Gourain et al., this issue) or after filtration using 0.2 µm filter
12 cartridges (Sartorius SARTOBRAN® 300) due to water budget restriction (Table 1). No significant difference was observed
13 between DFe values filtered through 0.2 µm and 0.45 µm filters (p-value > 0.2, Wilcoxon test) for most stations. Differences
14 were only observed between profiles of stations 11 and 13 and, 13 and 15. Seawater was collected in acid-cleaned 60 mL
15 LDPE bottles, after rinsing 3 times with about 20 mL of seawater. Teflon® tubing used to connect the filter holders or cartridges
16 to the GO-FLO bottles were washed in an acid-bath (10% v/v HCl, Suprapur®, Merck) for at least 12 h and rinsed three times
17 with Ultra High Purity Water (UHPW > 18 MΩ.cm) prior to use. Samples were then acidified to ~ pH 1.7 with HCl (Ultrapur®
18 Merck, 2 ‰ v/v) under a class 100 laminar flow hood inside the clean container. The sample bottles were then double bagged
19 and stored at ambient temperature in the dark before shore-based analyses.

20 Large volumes of seawater sample (referred hereafter as the in-house standard seawater) were also collected using a towed
21 fish at around 2-3 m deep and filtered in-line inside a clean container through a 0.2 µm pore size filter capsule (Sartorius
22 SARTOBRAN® 300) and was stored unacidified in 20-30 L LDPE carboys (Nalgene™). All the carboys were cleaned
23 following the guidelines of the GEOTRACES Cookbook (Cutter et al., 2017). This in-house standard seawater was used for
24 calibration on the SeaFAST-pico™ - SF-ICP-MS (see Section 2.2) and was acidified to ~ pH 1.7 with HCl (Ultrapur® Merck,
25 2 ‰ v/v) at least 24h prior to analysis.

26 **2.2 DFe analysis with SeaFAST-pico™**

27 Seawater samples were preconcentrated using a SeaFAST-pico™ (ESI, Elemental Scientific, USA) and the eluent was directly
28 introduced via a PFA-ST nebulizer and a cyclonic spray chamber in an Element XR Sector Field Inductively Coupled Plasma
29 Mass Spectrometry (Element XR SF-ICP-MS, Thermo Fisher Scientific Inc., Omaha, NE), following the protocol of
30 Lagerström et al. (2013).

31 High-purity grade solutions and water (Milli-Q) were used to prepare the following reagents each day: the acetic acid-
32 ammonium acetate buffer (CH₃COO⁻ and NH₄⁺) was made of 140 mL acetic acid (> 99% NORMATOM® - VWR chemicals)
33 and ammonium hydroxide (25%, Merck Suprapur®) in 500 mL PTFE bottles and was adjusted to pH 6.0 ± 0.2 for the on-line

1 pH adjustment of the samples. The eluent was made of 1.4 M nitric acid (HNO₃, Merck Ultrapur®) in Milli-Q water by a 10-
2 fold dilution and spiked with 1 µg L⁻¹ ¹¹⁵In (SCP Science calibration standards) to allow for drift correction. Autosampler and
3 column rinsing solutions were made of HNO₃ 2.5% (v/v) (Merck Suprapur®) in Milli-Q water. The carrier solution driven by
4 the syringe pumps to move the sample and buffer through the flow injection system was made in the same way.
5 All reagents, standards, samples, and blanks were prepared in acid cleaned low density polyethylene (LDPE) or Teflon
6 fluorinated ethylene propylene (FEP) bottles. Bottles were cleaned following the GEOTRACES protocol (Cutter et al., 2017).
7 Mixed element standard solution was prepared gravimetrically using high purity standards (Fe, Mn, Cd, Co, Zn, Cu, Pb; SCP
8 Science calibration standards) in HNO₃ 3% (v/v) (Merck Ultrapur®). A six-point calibration curve was prepared by standard
9 additions of the mixed element standard to our acidified in-house standard and ran at the beginning, the middle and the end of
10 each analytical session. The distribution of the trace metals other than Fe will be reported elsewhere (Planquette et al., in prep.).
11 Final concentrations of samples and procedural blanks were calculated from In-normalized data. Data were blank-corrected
12 by subtracting an average acidified Milli-Q blank that were pre-concentrated on the SeaFAST-pico™ in the same way as the
13 samples and seawater standards. Each analytical session consisted of about fifty samples and two calibrations, one at the
14 beginning and another one at the end of each analytical session. The errors associated to each sample were calculated as the
15 standard deviation for five measurements of low-Fe seawater samples. The mean Milli-Q blank was equal to 0.08 ± 0.09 nmol
16 L⁻¹ (n = 17) all analytical session together. The detection limit, calculated for a given run as three times the standard deviation
17 of the Milli-Q blanks, was on average 0.05 ± 0.05 nmol L⁻¹ (n = 17). Reproducibility was assessed through the standard
18 deviation of replicate samples (every 10th sample was a replicate) and the average of the in-house standard seawater, and was
19 equal to 17% (n = 84). Accuracy was determined from the analysis of consensus (SAFe S, GSP) and certified (NASS-7)
20 seawater matrices (see Table 2) and in-house standard seawater (DFe = 0.42 ± 0.07 nmol L⁻¹, n = 84). Note that all the DFe
21 values were generated in nmol kg⁻¹ using the SeaFAST-pico™ coupled to an Element XR SF-ICP-MS and were converted to
22 nmol L⁻¹ (multiplied by a factor of 1.025 kg L⁻¹) to be directly comparable with literature.

23 **2.3 Meteoric water and sea ice fraction calculation**

24 We separated the mass contributions to samples from stations 53, 61 and 78 in Sea-Ice Melt (SIM) Meteoric Water (MW) and
25 saline seawater inputs using the procedure and mass balance calculations that are fully described in Benetti et al. (2016).
26 Hereafter, we describe briefly the principle. We considered two types of seawater, namely the Atlantic Water (AW) and the
27 Pacific Water (PW). After estimating the relative proportions of AW (f_{AW}) and PW (f_{PW}) and their respective salinity and
28 $\delta^{18}\text{O}$ affecting each samples, the contribution of SIM and MW can be determined using measured salinity (S_m) and $\delta^{18}\text{O}$
29 (δO_m^{18}). The mass balance calculations are presented below:

$$30 \quad f_{AW} + f_{PW} + f_{MW} + f_{SIM} = 1 \text{ (eq.1)}$$

$$31 \quad f_{AW} \cdot S_{AW} + f_{PW} \cdot S_{PW} + f_{MW} \cdot S_{MW} + f_{SIM} \cdot S_{SIM} = S_m \text{ (eq.2)}$$

$$32 \quad f_{AW} \cdot \delta\text{O}_{AW}^{18} + f_{PW} \cdot \delta\text{O}_{PW}^{18} + f_{MW} \cdot \delta\text{O}_{MW}^{18} + f_{SIM} \cdot \delta\text{O}_{SIM}^{18} = \delta\text{O}_m^{18} \text{ (eq.3)}$$

1 where f_{AW} , f_{PW} , f_{MW} , f_{SIM} are the relative fraction of AW, PW, MW, and SIM. To calculate the relative fractions of AW, PW,
2 MW and SIM we used the following end-members: $S_{AW} = 35$, $\delta O_{AW}^{18} = +0.18\text{‰}$ (Benetti et al., 2016); $S_{PW} = 32.5$, $\delta O_{PW}^{18} = -$
3 1‰ (Cooper et al., 1997; Woodgate and Aagaard, 2005); $S_{MW} = 0$, $\delta O_{MW}^{18} = -18.4\text{‰}$ (Cooper et al., 2008); $S_{SIM} = 4$, $\delta O_{SIM}^{18} =$
4 $+0.5\text{‰}$ (Melling and Moore, 1995).
5 Negative sea-ice fractions indicated a net brine release while positive sea-ice fractions indicated a net sea-ice melting. Note
6 that for stations over the Greenland Shelf, we assumed that the Pacific Water (PW) contribution was negligible for the
7 calculations, supported by the very low PW fractions found at Cape Farewell in May 2014 (see Figure B1 in Benetti et al.,
8 2017), while for station 78, located on the Newfoundland shelf, we used nutrient measurements to calculate the PW fractions,
9 following the approach from Jones et al. (1998) (the data are published in Benetti et al., 2017).

10 **2.4 Ancillary measurements and mixed layer depth determination**

11 Potential temperature (θ), salinity (S), dissolved oxygen (O_2) and beam attenuation data were retrieved from the CTD sensors
12 (CTD SBE911 equipped with a SBE-43) that were deployed on a stainless steel rosette. Nutrient and pigment samples were
13 obtained from the stainless steel rosette casts and analysed according to Aminot and Kerouel (2007) and Ras et al. (2008),
14 respectively. We used the data from the stainless steel rosette casts that were deployed immediately before or after our TMR
15 casts. All these data are available on the LEFE/CYBER database (<http://www.obs-vlfr.fr/proof/php/geovide/geovide.php>).
16 The mixed layer depth (Z_m) for each station was calculated using the function “calculate.mld” (part of the “rcalcofi” package,
17 Ed Weber at NOAA SWFSC) created by Sam McClathie (NOAA Federal, 30th December 2013) for R software and where Z_m
18 is defined as an absolute change in the density of seawater at a given temperature ($\Delta\sigma_\theta \geq 0.125 \text{ kg m}^{-3}$) with respect to an
19 approximately uniform region of density just below the ocean surface (Kara et al., 2000). In addition to the density criterion,
20 the temperature and salinity profiles were inspected at each station for uniformity within this layer. When they were not
21 uniform, the depth of any perturbation in the profile was chosen as the base of the Z_m (Table 1).

22 **2.5 Statistical analysis**

23 All statistical approaches, namely the comparison between the pore size used for filtration, correlations and Principal
24 Component Analysis (PCA), were performed using the R statistical software (R development Core Team 2012). For all the
25 results, p-values were calculated against the threshold value alpha (α), that we assigned at 0.05, corresponding to a 95% level
26 of confidence. For all data sets, non-normal distributions were observed according to the Shapiro-Wilk test. Therefore, the
27 significance level was determined with a Wilcoxon test.

28 All sections and surface layer plots were prepared using Ocean Data View (Schlitzer, 2016).

1 **2.6 Water mass determination and associated DFe concentrations**

2 The water mass structure in the North Atlantic Ocean from the GEOVIDE voyage was quantitatively assessed by means of an
3 extended Optimum Multi-Parameter (eOMP) analysis with 14 water masses (for details see García-Ibáñez et al., 2015; this
4 issue). Using this water mass determination, DFe concentrations were considered as representative of a specific water mass
5 only when the contribution of this specific water mass was higher than 60% of the total water mass pool.
6

7 **2.7 Database**

8 The complete database of dissolved Fe is available in the electronic supplement www.biogeosciences.net. Overall, 540 data
9 points of dissolved Fe are reported, among which 511 values are used in this manuscript. The remaining 29 values (5.7% of
10 the total dataset) are flagged as (suspect) outliers. These 29 outliers were not used in figures and in the interpretation of this
11 manuscript. The criteria for rejection were based on the comparison with other parameters measured from the same GO-FLO
12 sampler, and curve fitting versus samples collected above and below the suspect sample. The complete data set will be available
13 in national and international databases (LEFE-CYBER, <http://www.obs-vlfr.fr/proof/index2.php>, and GEOTRACES
14 <http://www.bodc.ac.uk/geotraces/>).

15 **3 Results**

16 **3.1 Hydrography**

17 The hydrology and circulation of the main water masses along the OVIDE section in the North Atlantic Subpolar Gyre and
18 their contribution to the Atlantic Meridional Overturning Circulation (AMOC) have been described using an eOMP analysis
19 by García-Ibáñez et al., (2015; this issue) and Zunino et al. (2017). For a schematic of water masses, currents and pathways,
20 see Daniault et al. (2016). Hereafter we summarise the main features (Fig. 1 and 2).
21

22 *Upper waters (~ 0 – 800 m)* - The cyclonic circulation of the Eastern North Atlantic Central Water (ENACW) ($12.3 < \theta <$
23 16°C , $35.66 < S < 36.2$, $241 < \text{O}_2 < 251 \mu\text{mol kg}^{-1}$) occupied the water column from 0 to ~ 800 m depth from stations 1 to 25
24 contributing to 60% of the water mass pool. The sharp Subarctic Front (between stations 26 and 29), caused by the northern
25 branch of the North Atlantic Current (NAC) separated the cyclonic subpolar from the anticyclonic subtropical gyre domains
26 at 50°N and 22.5°W . The ENACW were also encountered to a lesser extent and only in surface waters (from 0 to ~ 100 m
27 depth) between stations 29 and 34 (contributing to less than 40% of the water mass pool). West of the Subarctic Front, Iceland
28 SubPolar Mode Waters (IcSPMW, $7.07 < \theta < 8^{\circ}\text{C}$, $35.16 < S < 35.23$, $280 < \text{O}_2 < 289 \mu\text{mol kg}^{-1}$) was encountered from
29 stations 34-40 (accounting for more than 45% of the water mass pool from 0 to ~ 800 m depth) and Irminger SubPolar Mode
30 Waters (IrSPMW, $\theta \approx 5^{\circ}\text{C}$, $S \approx 35.014$) from stations 42-44 (contributing to 40% of the water mass pool from 0 to ~ 250 m

1 depth) and stations 49 and 60 (accounting for 40% of the water mass pool down to 1300 m depth). The IcSPMW was also
2 observed within the Subtropical gyre (stations 11-26), subducted below ENACW until ~ 1000 m depth. Stations 63 (> ~ 200
3 m depth) and 64 (from surface down to ~ 500 m depth) exhibited a contribution of the IrSPMW higher than 45%. Stations 44,
4 49 and 60, from the Irminger Sea, and 63 from the Labrador Sea were characterised by lower sea-surface salinity ranges ($S =$
5 $[34.636, 34.903]$, stations 63 and 60, respectively). Subarctic Intermediate Water (SAIW, $4.5 < \theta < 6.0^{\circ}\text{C}$, $34.70 < S < 34.80$)
6 contributed to more than 40% of the water mass pool in the Iceland Basin between the surface and ~ 400 m depth at stations
7 29 and 32 and throughout the water column of stations 53, 56 and 61 and from surface down to ~ 200 m depth at station 63.
8 From stations 68 to 78 surface waters were characterized by a minimum of salinity and a maximum of oxygen ($S = 34.91$, O_2
9 $= 285 \mu\text{mol kg}^{-1}$, $\theta \approx 3^{\circ}\text{C}$) and corresponded to the newly formed Labrador Sea Water (LSW). The LSW was also observed in
10 surface waters of station 44 with a similar contribution than IrSPMW (~ 40%).

11

12 *Intermediate waters (~ 800 – 1400 m)* - The Mediterranean Outflow Water (MOW), distinguishable from surrounding Atlantic
13 Water by its high salinity tongue (up to 36.2), a minimum of oxygen ($\text{O}_2 = 210 \mu\text{mol kg}^{-1}$) and relatively high temperatures
14 (up to 11.7°C) was observed from station 1 to 21 between 800 and 1400 m depth at a neutral density ranging from 27.544 to
15 27.751 kg m^{-3} with the maximum contribution to the whole water mass pool seen at station 1 ($64 \pm 6\%$). Its main core was
16 located at ~ 1200 m depth off the Iberian shelf from stations 1 to 11 and then gradually rising westward due to mixing with
17 LSW within the North Atlantic subtropical gyre and a contribution of this water mass decreasing until station 21 down to 10-
18 20%. The LSW ($27.763 < \text{neutral density} < 27.724 \text{ kg m}^{-3}$) was sourced from the SPMW after intense heat loss and led to its
19 deep convection. During GEOVIDE, LSW formed by deep convection the previous winter was found at several stations in the
20 Labrador Sea (68, 69, 71 and 77). After convecting, LSW splits into three main branches with two main cores separated by the
21 Reykjanes Ridge (stations 1-32, West European and Iceland Basins; stations 40-60, Irminger Sea), and the last one entering
22 the West European Basin (Zunino et al., 2017).

23

24 *Overflows and Deep waters (~ 1400 - 5500 m)* - North East Atlantic Deep Water (NEADW, $1.98 < \theta < 2.50^{\circ}\text{C}$, $34.895 < S <$
25 34.940) was the dominant water mass in the West European Basin at stations 1-29 from 2000 m depth to the bottom and is
26 characterized by high silicic acid ($42 \pm 4 \mu\text{mol L}^{-1}$), nitrate ($21.9 \pm 1.5 \mu\text{mol L}^{-1}$) concentrations and lower oxygen concentration
27 ($\text{O}_2 \approx 252 \mu\text{mol kg}^{-1}$) (see Sarthou et al., 2018). The core of the NEADW (stations 1-13) was located near the seafloor and
28 gradually decreased westward. Polar Intermediate Water (PIW, $\theta \approx 0^{\circ}\text{C}$, $S \approx 34.65$) is a ventilated, dense, low-salinity water
29 intrusion to the deep overflows within the Irminger and Labrador Seas that is formed at the Greenland shelf. PIW represents
30 only a small contribution to the whole water mass pool (up to 27%) and was observed over the Greenland slope at stations 53
31 and 61 as well as in surface waters from station 63 (from 0 to ~ 200 m depth), in intermediate waters of stations 49, 60 and 63
32 (from ~ 500 to ~ 1500 m depth) and in bottom waters of stations 44, 68, 69, 71 and 77 with a contribution higher than 10%.
33 Iceland Scotland Overflow Water (ISOW, $\theta \approx 2.6^{\circ}\text{C}$, $S \approx 34.98$) is partly formed within the Arctic Ocean by convection of the
34 modified Atlantic water. ISOW comes from the Iceland-Scotland sills and flows southward towards the Charlie-Gibbs Fracture

1 Zone (CGFZ) and Bight Fracture Zone (BFZ) (stations 34 and 36) after which it reverses its flowing path northward and enters
2 the Irminger Sea (stations 40 and 42) to finally reach the Labrador Sea close to the Greenland coast (station 49, station 44
3 being located in between this two opposite flow paths). Along the eastern (stations 26-36) and western (stations 40-44) flanks
4 of the Reykjanes Ridge, ISOW had a contribution higher than 50% to the water mass pool. ISOW was observed from 1500 m
5 depth to the bottom of the entire Iceland Basin (stations 29-38) and from 1800 to 3000 m depth within the Irminger Sea
6 (stations 40-60). ISOW, despite having a fraction lower than 45% above the Reykjanes Ridge (station 38), was the main
7 contributor to the water mass pool from 1300 m depth down to the bottom. ISOW was also observed within the Labrador Sea
8 from stations 68 to 77. Finally, the deepest part of the Irminger (stations 42 and 44) and Labrador (stations 68-71) Seas were
9 occupied by Denmark Strait Overflow Water (DSOW, $\theta \approx 1.30^{\circ}\text{C}$, $S \approx 34.905$).

10 **3.2 Ancillary data**

11 **3.2.1 Nitrate**

12 Surface nitrate (NO_3^-) concentrations (García-Ibáñez et al., 2018; Pérez et al., 2018; Sarthou et al., 2018) ranged from 0.01 to
13 $10.1 \mu\text{mol L}^{-1}$ (stations 53 and 63, respectively). There was considerable spatial variability in NO_3^- surface distributions with
14 high concentrations found in the Iceland Basin and Irminger Sea (higher than $6 \mu\text{mol L}^{-1}$), as well as at stations 63 ($10.1 \mu\text{mol}$
15 L^{-1}) and 64 ($5.1 \mu\text{mol L}^{-1}$), and low concentrations observed in the West European Basin, in the Labrador Sea and above
16 continental margins. The low surface concentrations in the West European Basin ranged from 0.02 (station 11) to 3.9 (station
17 25) $\mu\text{mol L}^{-1}$. Station 26 delineating the extreme western boundary of the West European Basin exhibited enhanced NO_3^-
18 concentrations as a result of mixing between ENACW and IcSPMW, although these surface waters were dominated by
19 ENACW. In the Labrador Sea (stations 68-78) low surface concentrations were observed with values ranging from 0.04 (station
20 68) to 1.8 (station 71) $\mu\text{mol L}^{-1}$. At depth, the lowest concentrations (lower than $15.9 \mu\text{mol L}^{-1}$) were measured in ENACW (~
21 0 - 800 m depth) and DSOW (> 1400 m depth), while the highest concentrations were measured within NEADW (up to 23.5
22 $\mu\text{mol L}^{-1}$), and in the mesopelagic zone of the West European and Iceland Basins (higher than $18.4 \mu\text{mol L}^{-1}$).

23 **3.2.2 Chlorophyll-*a***

24 Overall, most of the phytoplankton biomass was localised above 100 m depth with lower total chlorophyll-*a* (TChl-*a*)
25 concentrations South of the Subarctic Front and higher at higher latitudes (see supplementary material Fig. S1). While
26 comparing TChl-*a* maxima considering all stations, the lowest value (0.35 mg m^{-3}) was measured within the West European
27 Basin (station 19, 50 m depth) while the highest values were measured at the Greenland (up to 4.9 mg m^{-3} , 30 m depth, station
28 53 and up to 6.6 mg m^{-3} , 23 m depth, station 61) and Newfoundland (up to 9.6 mg m^{-3} , 30 m depth, station 78) margins.

1 **3.3 Dissolved Fe concentrations**

2 Dissolved Fe concentrations (see supplementary material Table S1) ranged from $0.09 \pm 0.01 \text{ nmol L}^{-1}$ (station 19, 20 m depth)
3 to $7.8 \pm 0.5 \text{ nmol L}^{-1}$ (station 78, 371 m depth) (see Fig. 3). Generally, vertical profiles of DFe for stations above the margins
4 (2, 4, 53, 56, 61, and 78) showed an increase with depth, although sea-surface maxima were observed at stations 2, 4 and 56.
5 For these margin stations, values ranged from 0.7 to 1.0 nmol L^{-1} in the surface waters. Concentrations increased towards the
6 bottom, with more than 7.8 nmol L^{-1} measured at station 78, approximately $1\text{-}3 \text{ nmol L}^{-1}$ for stations 2, 4, 53, and 61, and just
7 above 0.4 nmol L^{-1} for station 56 (Fig. 4). Considering the four oceanic basins, mean vertical profiles (supplementary material
8 Fig. S2) showed increasing DFe concentrations down to 3000 m depth followed by decreasing DFe concentrations down to
9 the bottom. Among deep-water masses, the lowest DFe concentrations were measured in the West European Basin. The
10 Irminger Sea displayed the highest DFe concentrations from 1000 m depth to the bottom relative to other basins at similar
11 depths (Fig. 4 and supplementary material Fig. S2). In the Labrador Sea, DFe concentrations were low and relatively constant
12 at about $0.87 \pm 0.06 \text{ nmol L}^{-1}$ from 250 m to 3000 m depth (Fig. S2). Overall, surface DFe concentrations were higher ($0.36 \pm$
13 0.18 nmol L^{-1}) in the North Atlantic Subpolar gyre (above 52°N) than in the North Atlantic Subtropical gyre ($0.17 \pm 0.05 \text{ nmol}$
14 L^{-1}). The upper surface DFe concentrations were generally smaller than 0.3 nmol L^{-1} , except for few stations in the Iceland
15 Basin (stations 32 and 38), Irminger (stations 40 and 42) and Labrador (station 63) Seas, where values ranged between $0.4\text{-}0.5$
16 nmol L^{-1} .

17

18 **3.4 Fingerprinting water masses**

19 In the Labrador Sea, IrSPMW exhibited an average DFe concentration of $0.61 \pm 0.21 \text{ nmol L}^{-1}$ ($n=14$). DFe concentrations in
20 the LSW were the lowest in this basin, with an average value of $0.71 \pm 0.27 \text{ nmol L}^{-1}$ ($n=53$) (see supplementary material Fig.
21 S3). Deeper, ISOW displayed slightly higher average DFe concentrations ($0.82 \pm 0.05 \text{ nmol L}^{-1}$, $n=2$). Finally, DSOW had the
22 lowest average ($0.68 \pm 0.06 \text{ nmol L}^{-1}$, $n=3$, see supplementary material Fig. S3) and median (0.65 nmol L^{-1}) DFe values for
23 intermediate and deep waters.

24 In the Irminger Sea, surface waters were composed of SAIW ($0.56 \pm 0.24 \text{ nmol L}^{-1}$, $n=4$) and IrSPMW ($0.72 \pm 0.32 \text{ nmol L}^{-1}$,
25 $n=34$). The highest open-ocean DFe concentrations (up to $2.5 \pm 0.3 \text{ nmol L}^{-1}$, station 44, 2600 m depth) were measured within
26 this basin. In the upper intermediate waters, LSW was identified only at stations 40 to 44, and had the highest DFe values with
27 an average of $1.2 \pm 0.3 \text{ nmol L}^{-1}$ ($n=14$). ISOW showed higher DFe concentrations than in the Iceland Basin ($1.3 \pm 0.2 \text{ nmol}$
28 L^{-1} , $n=4$). At the bottom, DSOW was mainly located at stations 42 and 44 and presented the highest average DFe values (1.4
29 $\pm 0.4 \text{ nmol L}^{-1}$, $n=5$) as well as the highest variability from all the water masses presented in this section (see supplementary
30 material Fig. S3).

31 In the Iceland Basin, SAIW and IcSPMW displayed similar averaged DFe concentrations ($0.67 \pm 0.30 \text{ nmol L}^{-1}$, $n=7$ and 0.55
32 $\pm 0.34 \text{ nmol L}^{-1}$, $n=22$, respectively). Averaged DFe concentrations were similar in both LSW and ISOW, and higher than in

1 SAIW and IcSPMW ($0.96 \pm 0.22 \text{ nmol L}^{-1}$, $n=21$ and $1.0 \pm 0.3 \text{ nmol L}^{-1}$, $n=10$, respectively, see supplementary material Fig.
2 S3).
3 Finally, in the West European Basin, DFe concentrations in ENACW were the lowest of the whole section with an average
4 value of $0.30 \pm 0.16 \text{ nmol L}^{-1}$ ($n=64$). MOW was present deeper in the water column but was not characterized by particularly
5 high or low DFe concentrations relative to the surrounding Atlantic waters (see supplementary material Fig. S3). The median
6 DFe value in MOW was very similar to the median value when considering all water masses (0.77 nmol L^{-1} , Fig. 3 and
7 supplementary material S3). LSW and IcSPMW displayed slightly elevated DFe concentrations compared to the overall
8 median with mean values of 0.82 ± 0.08 ($n=28$) and 0.80 ± 0.04 ($n=8$) nmol L^{-1} , respectively. The DFe concentrations in
9 NEADW were relatively similar to the DFe median value of the GEOVIDE voyage (median DFe = 0.75 nmol L^{-1} , Fig. 3 and
10 supplementary material Fig. S3) with an average value of $0.74 \pm 0.16 \text{ nmol L}^{-1}$ ($n=18$) and presented relatively low median
11 DFe concentrations (median DFe = 0.71 nmol L^{-1}) compared to other deep water masses.

12 **4 Discussion**

13 In the following sections, we will first discuss the high DFe concentrations observed throughout the water column of stations
14 1 and 17 located in the West European Basin (Section 4.1), then, the relationship between water masses and the DFe
15 concentrations (Section 4.2) in intermediate (Section 4.2.2 and 4.2.3) and deep (Section 4.2.4 and 4.2.5) waters. We will also
16 discuss the role of wind (Section 4.2.1), rivers (Section 4.3.1), meteoric water and sea-ice processes (Section 4.3.2),
17 atmospheric deposition (Section 4.3.3) and sediments (Section 4.4) in delivering DFe. Finally, we will discuss the potential Fe
18 limitation using DFe:NO₃⁻ ratios (Section 4.5).

19 **4.1 High DFe concentrations at station 1 and 17**

20 Considering the entire section, two stations (stations 1 and 17) showed irregularly high DFe concentrations ($> 1 \text{ nmol L}^{-1}$)
21 throughout the water column, thus suggesting analytical issues. However, these two stations were analysed twice and provided
22 similar results, therefore discarding any analytical issues. This means that these high values originated either from genuine
23 processes or from contamination issues. If there had been contamination issues, one would expect a more random distribution
24 of DFe concentrations and less consistence throughout the water column. It thus appears that contamination issues were
25 unlikely to happen. Similarly, the influence of water masses to explain these distributions was discarded as the observed high
26 homogenized DFe concentrations were restricted to these two stations. Station 1, located at the continental shelf-break of the
27 Iberian Margin, also showed enhanced PFe concentrations from lithogenic origin suggesting a margin source (Gourain et al.,
28 2018). Conversely, no relationship was observed between DFe and PFe nor transmissometry for station 17. However, Ferron
29 et al. (2016) reported a strong dissipation rate at the Azores-Biscay Rise (station 17) due to internal waves. The associated
30 vertical energy fluxes could explain the homogenized profile of DFe at station 17, although such waves are not clearly
31 evidenced in the velocity profiles. Consequently, the elevated DFe concentrations observed at station 17 remain unsolved.

1 **4.2 DFe and hydrology keypoints**

2 **4.2.1 How do Air-sea interactions affect DFe concentration in the Irminger Sea?**

3 Among the four distinct basins described in this paper, the Irminger Sea exhibited the highest DFe concentrations within the
4 surface waters (from 0 to 250 m depth) with values ranging from 0.23 to 1.3 nmol L⁻¹ for open-ocean stations. Conversely,
5 low DFe concentrations were previously reported in the central Irminger Sea by Rijkenberg et al. (2014) (April-May, 2010)
6 and Achterberg et al. (2018) (April-May and July-August, 2010) with DFe concentrations ranging from 0.11 to 0.15 and from
7 ~ 0 to 0.14 nmol L⁻¹, respectively (see supplementary material Fig. S4 and Table S2). Differences might be due to the
8 phytoplankton bloom advancement, the high remineralization rate (Lemaître et al., 2017) observed within the LSW in the
9 Irminger Sea (see Section 4.1.3) and a deeper winter convection in early 2014. Indeed, enhanced surface DFe concentrations
10 measured during GEOVIDE in the Irminger Sea could be due to intense wind forcing events that would deepen the winter Z_m
11 down to the core of the Fe-rich LSW.

12 In the North Atlantic Ocean, the warm and salty water masses of the upper limb of the MOC are progressively cooled and
13 become denser, and subduct into the abyssal ocean. In some areas of the SubPolar North Atlantic, deep convective winter
14 mixing provides a rare connection between surface and deep waters of the MOC thus constituting an important mechanism in
15 supplying nutrients to the surface ocean (de Jong et al., 2012; Louanchi and Najjar, 2001). Deep convective winter mixing is
16 triggered by the effect of wind and a pre-conditioning of the ocean in such a way that the inherent stability of the ocean is
17 minimal. Pickart et al. (2003) demonstrated that these conditions are satisfied in the Irminger Sea with the presence of weakly
18 stratified surface water, a close cyclonic circulation, which leads to the shoaling of the thermocline and intense winter air-sea
19 buoyancy fluxes (Marshall and Schott, 1999). Moore (2003) and Piron et al. (2016) described low-level westerly jets centred
20 northeast of Cape Farewell, over the Irminger Sea, known as tip jet events. These events occur when wind is split around the
21 orographic features of Cape Farewell, and are strong enough to induce deep convective mixing (Bacon et al., 2003; Pickart et
22 al., 2003). It has also been shown that during winters with a positive North Atlantic Oscillation (NAO) index, the occurrence
23 of such events is favoured (Moore, 2003; Pickart et al., 2003), which was the case in the winter 2013-2014, preceding the
24 GEOVIDE voyage as opposed to previous studies (Lherminier, pers. comm.). The winter mixed layer depth prior to the cruise
25 reached up to 1200 m depth in the Irminger Sea (Zunino et al., 2017), which was most likely attributed to a final deepening
26 due to wind forcing events (centred at station 44). Such winter entrainment was likely the process involved in the vertical
27 supply of DFe within surface waters fuelling the spring phytoplankton bloom with DFe values close to those found in LSW.

28 **4.2.2 Why don't we see a DFe signature in the Mediterranean Overflow Water (MOW)?**

29 On its northern shores, the Mediterranean Sea is bordered by industrialized European countries, which act as a continuous
30 source of anthropogenic derived constituents into the atmosphere, and on the southern shores by the arid and desert regions of
31 north African and Arabian Desert belts, which act as sources of crustal material in the form of dust pulses (Chester et al., 1993;
32 Guerzoni et al., 1999; Martin et al., 1989). During the summer, when thermal stratification occurs, DFe concentrations in the

1 SML can increase over the whole Mediterranean Sea by 1.6-5.3 nmol L⁻¹ in response to the accumulation of atmospheric Fe
2 from both anthropogenic and natural origins (Bonnet and Guieu, 2004; Guieu et al., 2010; Sarthou and Jeandel, 2001). After
3 atmospheric deposition, the fate of Fe will depend on the nature of aerosols, vertical mixing, biological uptake and scavenging
4 processes (Bonnet and Guieu, 2006; Wuttig et al., 2013). During GEOVIDE, MOW was observed from stations 1 to 29
5 between 1000 and 1200 m depth and associated with high dissolved aluminium (DAI, Menzel Barraqueta et al., 2018)
6 concentrations (up to 38.7 nmol L⁻¹), confirming the high atmospheric deposition in the Mediterranean region. In contrast to
7 Al, no DFe signature was associated with MOW (Figs. 2 and 3). This feature was also reported in some studies (Hatta et al.,
8 2015; Thuróczy et al., 2010), while others measured higher DFe concentrations in MOW (Gerringa et al., 2017; Sarthou et al.,
9 2007). However, MOW coincides with the maximum Apparent Oxygen Utilization (AOU) and it is not possible to distinguish
10 the MOW signal from the remineralisation one (Sarthou et al., 2007). On the other hand, differences between studies are likely
11 originating from the intensity of atmospheric deposition and the nature of aerosols. Indeed, Wagener et al. (2010) highlighted
12 that large dust deposition events can accelerate the export of Fe from the water column through scavenging. As a result, in
13 seawater with high DFe concentrations and where high dust deposition occurs, a strong individual dust deposition event could
14 act as a sink for DFe. It thus becomes less evident to observe a systematic high DFe signature in MOW despite dust inputs.

15 **4.2.3 Fe enrichment in Labrador Sea Water (LSW)**

16 As described in Section 3.1, the LSW exhibited increasing DFe concentrations from its source area, the Labrador Sea, toward
17 the other basins with the highest DFe concentrations observed within the Irminger Sea, suggesting that the water mass was
18 enriched in DFe either locally in each basin or during its flow path (see supplementary material Fig. S3). These DFe sources
19 could originate from a combination of high export of PFe and its remineralisation in the mesopelagic area and/or the dissolution
20 of sediment.

21 The Irminger and Labrador Seas exhibited the highest averaged integrated TChl-*a* concentrations (98 ± 32 mg m⁻² and 59 ± 42
22 mg m⁻²) compared to the West European and Iceland Basins (39 ± 10 mg m⁻² and 53 ± 16 mg m⁻²), when the influence of
23 margins was discarded. Stations located in the Irminger (stations 40-56) and Labrador (stations 63-77) Seas, were largely
24 dominated by diatoms (>50% of phytoplankton abundances) and displayed the highest chlorophyllid-*a* concentrations, a tracer
25 of senescent diatom cells, likely reflecting post-bloom condition (Tonnard et al., in prep.). This is in line with the highest POC
26 export data reported by Lemaitre et al. (2018) in these two oceanic basins. This likely suggests that biogenic PFe export was
27 also higher in the Labrador and Irminger Seas than in the West European and Iceland Basins. In addition, Gourain et al. (2018)
28 highlighted a higher biogenic contribution for particles located in the Irminger and Labrador Seas with relatively high PFe:PAI
29 ratios (0.44 ± 0.12 mol:mol and 0.38 ± 0.10 mol:mol, respectively) compared to particles from the West European and Iceland
30 Basins (0.22 ± 0.10 and 0.38 ± 0.14 mol:mol, respectively, see Fig. 6 in Gourain et al., 2018). However, they reported no
31 difference in PFe concentrations between the four oceanic basins (see Fig. 12A in Gourain et al., 2018) when the influence of
32 margins was discarded, which likely highlighted the remineralisation of PFe within the Irminger and Labrador Seas. Indeed,
33 Lemaître et al. (2017) reported higher remineralisation rates within the Labrador (up to 13 mmol C m⁻² d⁻¹) and Irminger Seas

1 (up to 10 mmol C m⁻² d⁻¹) using the excess barium proxy (Dehairs et al., 1997), compared to the West European and Iceland
2 Basins (ranging from 4 to 6 mmol C m⁻² d⁻¹). Therefore, the intense remineralisation rates measured in the Irminger and
3 Labrador Seas likely resulted in enhanced DFe concentrations within LSW.
4 Higher DFe concentrations were, however, measured in the Irminger Sea compared to the Labrador Sea and coincided with
5 lower transmissometry values (i.e. 98.0-98.5% vs. >99%), thus suggesting a particle load of the LSW. This could be explained
6 by the reductive dissolution of Newfoundland Margin sediments. Indeed, Lambelet et al. (2016) reported high dissolved
7 neodymium (Nd) concentrations (up to 18.5 pmol.kg⁻¹) within the LSW at the edge of the Newfoundland Margin (45.73°W,
8 51.82°N) as well as slightly lower Nd isotopic ratio values relative to those observed in the Irminger Sea. They suggested that
9 this water mass had been in contact with sediments approximately within the last 30 years (Charette et al., 2015). Similarly,
10 during GA03, Hatta et al. (2015) attributed the high DFe concentrations in the LSW to continental margin sediments.
11 Consequently, it is also possible that the elevated DFe concentrations from the three LSW branches which entered the West
12 European and Iceland Basins and Irminger Sea was supplied through sediment dissolution (Measures et al., 2013) along the
13 LSW pathway.
14 The enhanced DFe concentrations measured in the Irminger Sea and within the LSW were thus likely attributed to the
15 combination of higher productivity, POC export and remineralisation as well as a DFe supply from reductive dissolution of
16 Newfoundland sediments to the LSW along its flow path.

17 **4.2.4 Enhanced DFe concentrations in the Irminger Sea bottom water**

18 Bottom waters from the Irminger Sea exhibited the highest DFe concentrations from the whole section, excluding the stations
19 at the margins. Such a feature could be due to i) vertical diffusion from local sediment, ii) lateral advection of water mass(es)
20 displaying enhanced DFe concentrations, and iii) local dissolution of Fe from particles. Hereafter, we discuss the plausibility
21 of these three hypotheses to occur.

22 The GEOTRACES GA02 voyage (leg 1, 64PE319) which occurred in April-May 2010 from Iceland to Bermuda sampled two
23 stations north and south of our station 44 (~ 38.95°W, 59.62°N): station 5 (~ 37.91°W, 60.43°N) and 6 (~ 39.71°W, 58.60°N),
24 respectively. High DFe concentrations in samples collected close to the bottom were also observed and attributed to sediment
25 inputs highlighting boundary exchange between seawater and surface sediment (Lambelet et al., 2016; Rijkenberg et al., 2014).
26 However, because a decrease in DFe concentrations was observed at our station 44 from 2500 m depth down to the bottom
27 (Fig. 3, see supplementary material Fig. S4 and Table S2), it appeared to be unlikely that these high DFe concentrations will
28 be the result of sediment inputs, as no DFe gradient from the deepest samples to those above was observed.

29 Looking at salinity versus depth for these three stations, one can observe the intrusion of Polar Intermediate Water (PIW) at
30 station 44 from GEOVIDE, which was not observed during the GA02 voyage and which contributed to about 14% of the water
31 mass composition (García-Ibáñez et al., this issue) and might therefore be responsible for the high DFe concentrations (see
32 supplementary material Fig. S5A). On the other hand, the PIW was also observed at station 49 (from 390 to 1240 m depth),
33 60 (from 440 to 1290 m depth), 63 (from 20 to 1540 m depth), 68 (3340 m depth), 69 (from 3200 to 3440 m depth), 71 (from

1 2950 to 3440 m depth) and 77 (60 and 2500 m depth) with similar or higher contributions of the PIW without such high DFe
2 concentrations (maximum DFe = 1.3 ± 0.1 nmol L⁻¹, 1240 m depth at station 49). However, considering the short residence
3 time of DFe and the circulation of water masses in the Irminger Sea, it is possible that instead of being attributed to one specific
4 water mass, these enhanced DFe concentrations resulted from lateral advection of the deep waters. Figure S5B) shows the
5 concentrations of both DFe and PFe for the mixing line between DSOW/PIW and ISOW at station 44 and considering 100%
6 contribution of ISOW for the shallowest sample (2218 m depth) and of DSOW/PIW for the deepest (2915 m depth), as these
7 were the main water masses. This figure shows increasing DFe concentrations as DSOW/PIW mixed with ISOW. In addition,
8 Le Roy et al. (2018) reported for the GEOVIDE voyage at station 44 a deviation from the conservative behaviour of ²²⁶Ra
9 reflecting an input of this tracer centred at 2500 m depth, likely highlighting diffusion from deep-sea sediments and coinciding
10 with the highest DFe concentrations measured at this station. Although the transmissometry data were lower at the sediment
11 interface than at 2500 m depth, Deng et al. (2018) reported a stronger scavenged component of the ²³⁰Th at the same depth
12 range, likely suggesting that the mixture of water masses were in contact with highly reactive particles. If there is evidence
13 that the enhanced DFe concentrations observed at station 44 coincided with lateral advection of water masses that were in
14 contact with particles, the difference of behaviour between DFe and ²³⁰Th remains unsolved. The only parameter that would
15 explain without any ambiguity such differences of behaviour between DFe and ²³⁰Th would be the amount of Fe-binding
16 organic ligands for these samples. Indeed, although PFe concentrations decreased from the seafloor to the above seawater, this
17 trend would likely be explained by a strong vertical diffusion alone and not necessarily by the dissolution of particles that were
18 laterally advected.
19 Therefore, the high DFe concentrations observed might be inferred from local processes as ISOW mixes with both PIW and
20 DSOW with a substantial load of Fe-rich particles that might have dissolved in solution due to Fe-binding organic ligands.

21 **4.2.5 Reykjanes Ridge: Hydrothermal inputs or Fe-rich seawater?**

22 Hydrothermal activity was assessed over the Mid Atlantic Ridge, namely the Reykjanes Ridge, from stations 36 to 40. Indeed,
23 within the interridge database (<http://www.interridge.org>), the Reykjanes Ridge is reported to have active hydrothermal sites.
24 The sites were either confirmed (Baker and German, 2004a; German et al., 1994; Olafsson et al., 1991; Palmer et al., 1995)
25 close to Iceland or inferred (e.g. Chen, 2003; Crane et al., 1997; German et al., 1994; Sinha et al., 1997; Smallwood and White,
26 1998) closer to the GEOVIDE section as no plume was detected but a high backscatter was reported potentially corresponding
27 to a lava flow. Therefore, hydrothermal activity at the sampling sites remains unclear with no elevated DFe concentrations nor
28 temperature anomaly above the ridge (station 38). However, enhanced DFe concentrations (up to 1.5 ± 0.22 nmol L⁻¹, station
29 36, 2200 m depth) were measured east of the Reykjanes Ridge (Fig. 3). This could be due to hydrothermal activity and
30 resuspension of sunken particles at sites located North of the section and transported through the ISOW towards the section
31 (see supplementary material Fig. S3). Indeed, Achterberg et al. (2018) highlighted at ~60°N and over the Reykjanes Ridge a
32 southward lateral transport of an Fe plume of up to 250-300 km. In agreement with these observations, previous studies (e.g.
33 Fagel et al., 1996; Fagel et al., 2001; Lackschewitz et al., 1996; Parra et al., 1985) reported marine sediment mineral clays in

1 the Iceland Basin largely dominated by smectite (> 60%), a tracer of hydrothermal alteration of basaltic volcanic materials
2 (Fagel et al., 2001; Tréguer and De La Rocha, 2013). Hence, the high DFe concentrations measured east of the Reykjanes
3 Ridge could be due to a hydrothermal source and/or the resuspension of particles and their subsequent dissolution.
4 West of the Reykjanes Ridge, a DFe-enrichment was also observed in ISOW within the Irminger Sea (Figs. 4 and 7). The low
5 transmissometer values within ISOW in the Irminger Sea compared to the Iceland Basin suggest a particle load. These particles
6 could come from the Charlie Gibbs Fracture Zone (CGFZ, 52.67°N and 34.61°W) and potentially Bight Fracture Zone (BFZ,
7 56.91°N and 32.74°W) (Fig. 1) (Lackschewitz et al., 1996; Zou et al., 2017). Indeed, hydrographic sections of the northern
8 valley of the CGFZ showed that below 2000 m depth the passage through the Mid-Atlantic Ridge was mainly filled with the
9 ISOW (Kissel et al., 2009; Shor et al., 1980). Shor et al. (1980) highlighted a total westward transport across the sill, below
10 2000 m depth of about $2.4 \times 10^6 \text{ m}^3 \text{ s}^{-1}$ with ISOW carrying a significant load of suspended sediment ($25 \mu\text{g L}^{-1}$), including a
11 100-m-thick benthic nepheloid layer. It thus appears that the increase in DFe within ISOW likely came from sediment
12 resuspension and dissolution as the ISOW flows across CGFZ and BFZ.

13 **4.3 What are the main sources of DFe in surface waters?**

14 During GEOVIDE, enhanced DFe surface concentrations were observed at several stations (stations 1-4, 53, 61, 78)
15 highlighting an external source of Fe to surface waters. The main sources able to deliver DFe to surface waters are riverine
16 inputs, glacial inputs and atmospheric deposition. In the following sections, these potential sources of DFe in surface waters
17 will be discussed.

18 **4.3.1 Tagus riverine inputs**

19 Enhanced DFe surface concentrations (up to $1.07 \pm 0.12 \text{ nmol L}^{-1}$) were measured over the Iberian Margin (stations 1-4) and
20 coincided with salinity minima ($\sim <35$) and enhanced DAi concentrations (up to 31.8 nmol L^{-1} , Menzel Barraqueta et al.,
21 2018). DFe and DAi concentrations were both significantly negatively correlated with salinity ($R^2 = \sim 1$ and 0.94, respectively)
22 from stations 1 to 13 (Fig. 5). Salinity profiles from station 1 to 4 showed evidence of a freshwater source with surface salinity
23 ranging from 34.95 (station 1) to 35.03 (station 4). Within this area, only two freshwater sources were possible: 1) wet
24 atmospheric deposition (4 rain events, Shelley, pers. comm.) and 2) the Tagus River, since the ship SADC data revealed a
25 northward circulation (P. Lherminier and P. Zunino, Ifremer Brest, pers. comm.). Our SML DFe inventories were about three
26 times higher at station 1 ($\sim 1 \text{ nmol L}^{-1}$) than those calculated during the GA03 voyage ($\sim 0.3 \text{ nmol L}^{-1}$, station 1) during which
27 atmospheric deposition were about one order of magnitude higher (Shelley et al., 2018; Shelley et al., 2015), the atmospheric
28 source seemed to be minor. Consequently, the Tagus River appears as the most likely source responsible for these enhanced
29 DFe concentrations, either as direct input of DFe or indirectly through Fe-rich sediment carried by the Tagus River and their
30 subsequent dissolution. The Tagus estuary is the largest in the western European coast and very industrialized (Canário et al.,
31 2003; de Barros, 1986; Figueres et al., 1985; Gaudencio et al., 1991; Mil-Homens et al., 2009), extends through an area of 320
32 km^2 and is characterized by a large water flow of $15.5 \cdot 10^9 \text{ m}^3 \text{ y}^{-1}$ (Fiuza, 1984). Many types of industry (e.g. heavy metallurgy,

1 ore processing, chemical industry) release metals including Fe, which therefore result in high levels recorded in surface
2 sediments, suspended particulate matter, water and organisms in the lower estuary (Santos-Echeandia et al., 2010).

3 **4.3.2 High latitude meteoric water and sea-ice processes**

4 Potential sources of Fe at stations 53, 61 and 78 include meteoric water (MW, referring to precipitation, runoff and continental
5 glacial melt), sea-ice melt (SIM), seawater interaction with shallow sediments and advection of water transported from the
6 Arctic sourced by the Fe-rich TransPolar Drift (TPD, Klunder et al. (2012); see supplementary material Fig. S4 and Table S2).
7 The vertical profiles of both potential temperature and salinity in the Greenland and Newfoundland Margins (station 53, 61
8 and 78, Fig. 4 D), E) and F)) highlighted the influence of fresh waters originating from the Arctic Ocean to separate surface
9 and deeper samples at ~ 60 m (station 53) and ~ 40 m (stations 61 and 78) depth. The presence of this freshwater lens suggests
10 that sediment derived enrichment to these surface waters was unlikely. The most plausible sources would be freshwater induced
11 by meteoric water and sea-ice melt. Deeper in the water column, net brine release were observed at stations 53 (below 40 m
12 depth, Fig. 4D) 61 (in the whole water column, Fig. 4E) and 78 (below 30 m depth, Fig. 4F). The release of brines could
13 originate from two different processes: the sea-ice formation or the early melting of multiyear sea ice due to gravitational
14 drainage and subsequent brine release (Petrich and Eicken, 2010; Wadhams, 2000). Indeed, during the winter preceding the
15 GEOVIDE voyage, multiyear sea ice extended 200 km far from our Greenland stations (<http://nsidc.org/arcticseaicenews/>). In
16 the following sections, we discuss the potential for meteoric water supply, sea-ice formation and sea-ice melting to affect DFe
17 distribution.

18

19 *4.3.2.1 The Greenland shelf*

20 Considering the sampling period at stations 53 (16 June 2014) and 61 (19 June 2014), sea-ice formation is unlikely to happen
21 as this period coincides with summer melting in both the Central Arctic and East Greenland (Markus et al., 2009). However,
22 it is possible that the brines observed in our study could originates from sea-ice formation, which occurred during the previous
23 winter(s) at 66°N (and/or higher latitudes). The residence time can vary from days (von Appen et al., 2014) to 6-9 months
24 (Sutherland et al., 2009). Due to our observed strong brine signal at station 61 we suggest that the residence time was potentially
25 longer than average. Given that the brine signal was higher at station 61 than at station 53 (which was located upstream in the
26 EGC), we suggest that station 53 was exhibiting a freshening as a result of the transition between the freezing period toward
27 the melting period. This would result in a dilution of the brine signal at the upstream station. Consequently, the salinity of this
28 brine signal may reflect sea ice formation versus melting which may have an effect on the trace metal concentration within
29 this water (Hunke et al., 2011). The associated brine water at station 61(100 m depth) was slightly depleted in both DFe and
30 PFe, which may be attributed to sea ice formation processes. Indeed, Janssens et al. (2016) highlighted that as soon as sea ice
31 forms, sea salts are efficiently flushed out of the ice while PFe is trapped within the crystal matrix and DFe accumulates,
32 leading to an enrichment factor of these two Fe fractions compared to underlying seawater. Conversely, the brine signal
33 observed at station 53 (100 m depth) showed slight enrichment in DFe, which may be attributed to brine release during early

1 sea ice melting and the associated release of DFe into the underlying water column as the brine sinks until reaching neutral
2 buoyancy due to higher density.

3 Surface waters (from 0 to ~ 100 m depth) from station 53 and 61 were characterized by high MW fractions (ranging from 8.3
4 to 7.4% and from 7.7 to 7.3% , respectively, from surface to ~100 m depth, Figs. 5D and E). These high MW fractions were
5 both enriched in PFe and DFe (except station 53 for which no data was available close to the surface) compared to seawater
6 located below 50 m depth, thus suggesting a MW source. These results are in line with previous observations, which
7 highlighted strong inputs of DFe from a meteoric water melting source in Antarctica (Annett et al., 2015). Although the ability
8 of MW from Greenland Ice Sheet and runoffs to deliver DFe and PFe to surrounding waters has previously been demonstrated
9 (Bhatia et al., 2013; Hawkings et al., 2014; Schroth et al., 2014; Statham et al., 2008), both Fe fractions were lower at the
10 sample closest to the surface, then reached a maximum at ~ 50 m depth and decreased at ~ 70 m depth, for station 61 (Fig.
11 4D). The surface DFe depletion was likely explained by phytoplankton uptake, as indicated by the high TChl-*a* concentrations
12 (up to 6.6 mg m⁻³) measured from surface to about 40 m depth, drastically decreasing at ~ 50 m depth to 3.9 mg m⁻³ (Fig. 4D).
13 Hence, it seemed that meteoric water inputs from the Greenland Margin likely fertilized surface waters with DFe, enabling the
14 phytoplankton bloom to subsist. The profile of PFe can be explained by two opposite plausible hypotheses: 1) MW inputs did
15 not release PFe, as if it was the case, one should expect higher PFe concentrations at the surface (~25 m depth) than the one
16 measured at 50 m depth due to both the release from MW and the assimilation of DFe by phytoplankton 2) MW inputs can
17 release PFe in a form that is directly accessible to phytoplankton with subsequent export of PFe as phytoplankton died. The
18 latter solution explains the PFe maximum measured at ~ 50 m depth and is thus the most plausible.

19

20 4.3.2.2 *The Newfoundland shelf*

21 Newfoundland shelf waters (station 78) were characterized by high MW fractions (up to 7%), decreasing from surface to 200
22 m depth (~2%). These waters were associated with a net sea-ice melting signal from the near surface to ~10 m depth followed
23 by a brine release signal down to 200 m depth with the maximum contribution measured at ~30 m depth. Within the surface
24 waters (above 20 m depth), no elevation in DFe, DA1 nor PFe was noticed despite the low measured TChl-*a* concentrations
25 (TChl-*a* ~ 0.20 mg m⁻³). This suggests that none of these inputs (sea-ice melting and meteoric water) were able to deliver DFe
26 or that these inputs were minor compared to sediment inputs from the Newfoundland Margin. Surprisingly, the highest TChl-
27 *a* biomass (TChl-*a* > 9 mg m⁻³) from the whole section was measured at 30 m depth corresponding to the strongest brine release
28 signal. This either suggests that the brine likely contained important amounts of Fe (dissolved and/or particulate Fe) that were
29 readily available for phytoplankton and consumed at the sampling period by potentially sea-ice algae themselves (Riebesell et
30 al., 1991) or that another nutrient was triggering the phytoplankton bloom.

31 4.3.3 Atmospheric deposition

32 On a regional scale, the North Atlantic basin receives the largest amount of atmospheric inputs due to its proximity to the
33 Saharan Desert (Jickells et al., 2005), yet even in this region of high atmospheric deposition, inputs are not evenly distributed.

1 Indeed, aerosol Fe loading measured during GEOVIDE (Shelley et al., 2017) were much lower (up to four orders of magnitude)
2 than those measured during studies from lower latitudes in the North Atlantic (e.g. Baker et al., 2013; Buck et al., 2010; and
3 for GA03, Shelley et al., 2015), but atmospheric inputs could still be an important source of Fe to surface waters in areas far
4 from land.

5 In an attempt to estimate whether there was enough atmospheric input to sustain the SML DFe concentrations, we calculated
6 Turnover Times relative to Atmospheric Deposition (TTADs, Guieu et al., 2014). To do so, we made the following
7 assumptions: 1) the aerosol concentrations are a snapshot in time but are representative of the study region, 2) the aerosol
8 solubility estimates based on two sequential leaches are an upper limit of the aerosol Fe in seawater and 3) the water column
9 stratified just before the deposition of atmospheric inputs, so MLD DFe will reflect inputs from above. Thus, the TTADs were
10 defined as the integrated DFe concentrations in the SML for each station divided by the contribution of soluble Fe contained
11 in aerosols averaged per basin to the water volume of the SML. Although, TTADs were lower in the West European and
12 Iceland Basins with an average of $\sim 9 \pm 3$ months compared to other basins (7 ± 2 years and 5 ± 2 years for the Irminger and
13 Labrador Seas, respectively) (Fig. 6) they were about three times higher than those reported for areas impacted by Saharan
14 dust inputs (~ 3 months, Guieu et al., 2014). Therefore, the high TTADs measured in the Irminger and Labrador Seas and
15 ranging from 2 to 15 years provided further evidence that atmospheric deposition were unlikely to supply Fe in sufficient
16 quantity to be the main source of DFe (see Sections 4.2.1 and 4.3.2) while in the West European and Iceland Basins they
17 played an additional source, perhaps the main source of Fe especially at station 36 which displayed TTAD of 3 months.

18 **4.4 Sediment input**

19 *4.4.1 Margins:*

20 DFe concentration profiles from all coastal stations (stations 2, 4, 53, 56, 61 and 78) are reported in Figure 4. To avoid surface
21 processes, only depths below 100 m depth will be considered in the following discussion. DFe and PFe followed a similar
22 pattern at stations 2, 53, 56, and 78 with increasing concentrations towards the sediment, suggesting that either the sources of
23 Fe supplied both Fe fractions (dissolved and particulate) or that PFe dissolution from sediments supplied DFe. Among the
24 different margins, the Newfoundland Margin exhibited the highest deep-water DFe concentrations. Conversely, stations 4 and
25 61 exhibited a decrease in DFe concentrations at the closest samples to the seafloor whereas PFe increased. DFe:PFe ratios
26 ranged from 0.01 (station 2, bottom sample) to 0.27 (station 4, ~ 400 m depth) mol:mol with an average value of 0.11 ± 0.07
27 mol:mol ($n = 23$, Table 3), highlighting a different behaviour of Fe among margins. This could be explained by the different
28 nature of the sediments and/or different sediment conditions (e.g. redox, organic content). Based on particulate and dissolved
29 Fe and dissolved Al data (Gourain et al., 2018; Menzel Barraqueta et al., 2018, Table 3), three main different types of margins
30 were reported (Gourain et al., 2018) with the highest lithogenic contribution observed at the Iberian Margin (stations 2 and 4)
31 and the highest biogenic contribution at the Newfoundland Margin (station 78). These observations are consistent with higher
32 TChl-*a* concentrations measured at the Newfoundland Margin and to a lesser extent at the Greenland Margin and the
33 predominance of diatoms relative to other functional phytoplankton classes at both margins (Tonnard et al., in prep.). To sum

1 up, the most biogenic sediments (Newfoundland Margin) were able to mobilise more Fe in the dissolved phase than the most
2 lithogenic sediments (Iberian Margin), in agreement with Boyd et al. (2010) who reported greater remineralization of PFe from
3 biogenic PFe than from lithogenic PFe based on field experiment and modelling simulations.

4

5 4.4.2 Nepheloid layers:

6 Samples associated with high levels of particles (transmissometer < 99%) and below 500 m depth displayed a huge variability
7 in DFe concentrations. From the entire dataset, 63 samples (~13% of the entire dataset) followed this criterion with 14 samples
8 from the West European Basin (station 1), 4 samples from the Iceland Basin (stations 29, 32, 36 and 38), 43 samples from the
9 Irminger Sea (stations 40, 42, 44, 49 and 60) and 2 samples from the Labrador Sea (station 69). To determine which parameter
10 was susceptible to explain the variation in DFe concentrations in these nepheloid layers, a Principal Component Analysis
11 (PCA) on these samples. The input variables of the PCA were the particulate Fe, Al, and particulate manganese (PMn) (Gourain
12 et al., 2018), the DAI (Menzel Barraqueta et al., 2018) and the Apparent Oxygen Utilization (AOU) and were all correlated to
13 DFe concentrations explaining all together 93% of the subset variance (see supplementary material Fig. S6). The first
14 dimension of the PCA was represented by the PAI, PFe and PMn concentrations and explained 59.5% of the variance, while
15 the second dimension was represented by the DAI and the AOU parameters, explaining 33.2% of the variance. The two sets
16 of variables were nearly at right angle from each other, indicating no correlation between them.

17 The variations in DFe concentrations measured in bottom samples from stations 32, 36 (Iceland Basin), 42 and 44 (Irminger
18 Sea) and 69 (Labrador Sea) were mainly explained by the first dimension of the PCA (see supplementary material Fig. S6).
19 Therefore, samples characterized by the lowest DFe concentrations (stations 32 and 69) were driven by particulate Al and Mn
20 concentrations and resulted in an enrichment of Fe within particles. These results are in agreement with previous studies
21 showing that the presence of Mn within particles can induce the formation of Fe-Mn oxides, contributing to the removal of Fe
22 and Mn from the water column (Kan et al., 2012; Teng et al., 2001).

23 Low DFe concentrations (bottom samples from stations 42 and 1) were linked to DAI inputs and associated with lower AOU
24 values. The release of Al has previously been observed from Fe and Mn oxide coatings on resuspended sediments under mildly
25 reducing conditions (Van Beusekom, 1988). Conversely, higher DFe concentrations were observed for stations 44 and 49 and
26 to a lesser extent station 60 coinciding with low DAI inputs and higher oxygen levels. This observation challenges the
27 traditional view of Fe oxidation with oxygen, either abiotically or microbially induced. Indeed, remineralisation can decrease
28 sediment oxygen concentrations, promoting reductive dissolution of PFe oxyhydroxides to DFe that can then diffuse across
29 the sediment water interface as DFe(II) colloids (Homoky et al., 2011). Such processes will inevitably lead to rapid Fe removal
30 through precipitation of nanoparticulate or colloidal Fe (oxyhydr)oxides, followed by aggregation or scavenging by larger
31 particles (Boyd and Ellwood, 2010; Lohan and Bruland, 2008) unless complexation with Fe-binding organic ligands occurs
32 (Batchelli et al., 2010; Gerringa et al., 2008). There exist, however, another process that is favoured in oxic benthic boundary
33 layers (BBL) with low organic matter degradation and/or low Fe oxides, which implies the dissolution of particles after
34 resuspension, namely the non-reductive dissolution of sediment (Homoky et al., 2013; Radic et al., 2011). In addition, these

1 higher oxygenated samples were located within DSOW, which mainly originate (75% of the overflow) from the Nordic Seas
2 and the Arctic Ocean (Tanhua et al., 2005), in which the ultimate source of Fe was reported by Klunder et al. (2012) to come
3 from Eurasian river waters. The major Arctic rivers were highlighted by Slagter et al. (2017) to be a source of Fe-binding
4 organic ligands that are then further transported via the TPD across the Denmark Strait. Hence, the enhanced DFe
5 concentrations measured within DSOW might result from Fe-binding organic ligand complexation that were transported to the
6 deep ocean as DSOW formed rather than the non-reductive dissolution of sediment.

7 **4.5 How does biological activity modify DFe distribution?**

8 Overall, almost all the stations from the GEOVIDE voyage displayed DFe minima in surface water associated with some
9 maxima of TChl-*a* (see supplementary material Fig. S1). In the following section, we specifically address the question of
10 whether DFe concentrations potentially limit phytoplankton growth. Note that macronutrients and DFe limitations relative to
11 phytoplankton functional classes are dealt in Tonnard et al. (in prep.).

12 A key determinant for assessing the significance of a DFe source is the magnitude of the DFe:macronutrient ratio supplied,
13 since this term determines to which extent DFe will be utilised. The DFe:NO₃⁻ ratios in surface waters varied from 0.02 (station
14 36) to 38.6 (station 61) mmol:mol with an average of 5 ± 10 mmol:mol (see supplementary material Fig. S7). Values were
15 typically equal or lower than 0.28 mmol mol⁻¹ in all basins except at the margins and at stations 11, 13, 68, 69 and 77. The low
16 nitrate concentrations observed at the eastern and western Greenland and Newfoundland Margins reflected a strong
17 phytoplankton bloom which had reduced the concentrations as highlighted by the elevated integrated TChl-*a* concentrations
18 ranging from 129.6 (station 78) to 398.3 (station 61) mg m⁻². At the Iberian Margin, they likely reflected the influence of the
19 N-limited Tagus River (stations 1, 2 and 4) with its low TChl-*a* integrated concentrations that ranged from 31.2 (station 1) to
20 46.4 (station 4) mg m⁻². The high DFe:NO₃⁻ ratios determined at those stations, which varied from 13.4 (station 78) to 38.6
21 (station 61) mmol:mol, suggested that waters from these areas, despite having the lowest NO₃⁻ concentrations, were relatively
22 enriched in DFe compared to waters from Iceland Basin and Irminger Sea.

23 In our study, DFe:NO₃⁻ ratios displayed a gradient from the West European Basin to Greenland (supplementary material S7
24 and S8). This trend only reverses when the influence of Greenland was encountered, as also observed by Painter et al. (2014).
25 The remineralisation of organic matter is a major source of macro and micronutrients in subsurface waters (from 50 to 250 m
26 depth). Remineralisation is associated with the consumption of oxygen and therefore, Apparent Oxygen Utilization (AOU)
27 can provide a quantitative estimate of the amount of material that has been remineralised. While no relationship was observed
28 below 50 m depth for NO₃⁻ or DFe and AOU considering all the stations, a significant correlation was found in the Subpolar
29 gyre when removing the influence of margins (stations 29-49, 56, 60, 63-77) ($\text{AOU} = 3.88 \text{ NO}_3^- - 39.32$, $R^2=0.79$, $n=69$, p -
30 value < 0.001). This correlation indicates that remineralisation of Particulate Organic Nitrogen (PON) greatly translates into
31 Dissolved Inorganic Nitrogen (DIN) and that NO₃⁻ can be used as a good tracer for remineralisation in the studied area. Within
32 these Subpolar gyre waters, there was a significant correlation between DFe and AOU ($\text{AOU} = 22.6 \text{ DFe}$, $R^2=0.34$, $n=53$, p -
33 value < 0.001). The open-ocean stations from Subpolar gyre also exhibited a good linear correlation between DFe and NO₃⁻

1 ($R^2=0.42$, $n=51$, p -value < 0.05). The slope of the relationship, representing the typical remineralisation ratio, was $R_{Fe:N} = 0.07$
2 ± 0.01 mmol mol⁻¹. The intercept of the regression line was -0.4 ± 0.2 mmol L⁻¹, reflecting possible excess of preformed NO₃⁻
3 compare to DFe in these water masses. These significant correlations allow us to use the Fe* tracer to assess where DFe
4 concentrations potentially limit phytoplankton growth by subtracting the contribution of organic matter remineralisation from
5 the dissolved Fe pool, as defined by Rijkenberg et al. (2014) and Parekh et al. (2005) for PO₄³⁻, and modified here for NO₃⁻ as
6 follow:

$$Fe^* = [DFe] - R_{Fe:N} \times [NO_3^-] \quad (\text{eq. 4})$$

7
8 where $R_{Fe:N}$ refers to the average biological uptake ratio Fe over nitrogen, and $[NO_3^-]$ refers to nitrate concentrations in
9 seawater. Although, we imposed a fixed biological $R_{Fe:N}$ of 0.05 mmol mol⁻¹, it is important to note that the biological uptake
10 ratio of DFe:NO₃⁻ is not likely to be constant. Indeed, this ratio has been found to range from 0.05 to 0.9 mmol mol⁻¹ depending
11 on species (Ho et al., 2003; Sunda and Huntsman, 1995; Twining et al., 2004). The ratio we choose is thus less drastic to assess
12 potential Fe limitation and more representative of the average biological uptake of DFe over NO₃⁻ calculated for this study (i.e.
13 $R_{Fe:N} = 0.07 \pm 0.01$ mmol mol⁻¹, for Subpolar waters). Negative values of Fe* indicate the removal of DFe that is faster than
14 the input through remineralisation or external sources and positive values suggest input of DFe from external sources (Fig. 7).
15 Consequently, figure 7 shows that phytoplankton communities with very high Fe requirements relative to NO₃⁻ ($R_{Fe:N} = 0.9$)
16 will only be able to grow above continental shelves where there is a high supply of DFe as previously reported by Nielsdóttir
17 et al. (2009) and Painter et al. (2014). All these results are corroborating the importance of the Tagus River (Iberian Margin,
18 see section 4.2.1), glacial inputs in the Greenland and Newfoundland Margins (see section 4.2.2) and to a lesser extent
19 atmospheric inputs (see section 4.2.3) in supplying Fe with Fe:N ratios higher than the average biological uptake/demand ratio.
20 Figure 7 (see also supplementary material S7, S8, S9 and S10) also highlights the Fe limitation for the low-Fe requirement
21 phytoplankton class ($R_{Fe:N} = 0.05$) within the Iceland Basin, Irminger and Labrador Seas. The Fe deficiency observed in surface
22 waters (> 50 m depth) from the Irminger and Labrador Seas might be explained by low atmospheric deposition for the IcSPMW
23 and the LSW (Shelley et al., 2017). Low atmospheric Fe supply and sub-optimal Fe:N ratios in winter overturned deep water
24 could favour the formation of the High-Nutrient, Low-Chlorophyll (HNLC) conditions. The West European Basin, despite
25 exhibiting some of the highest DFe:NO₃⁻ ratios within surface waters (see supplementary material Fig. S8), displayed the
26 strongest Fe-depletion from 50 m depth down to the bottom, suggesting that the main source of Fe was coming from dust
27 deposition and/or riverine inputs.

28 Similarly as for the West European Basin, the pattern displayed in the surface map of DFe:NO₃⁻ ratios (supplementary material
29 S8) extended to about 50 m depth, after which the trend reversed (Fig. 7 and supplementary material Fig. S7). Below 50 m
30 depth, the Fe* tracer (Fig. 7) was positive in the Irminger Sea and overall negative in the other basins. In the Irminger Sea
31 positive Fe* values were likely the result of the winter entrainment of Fe-rich LSW (see section 4.2.1) coinciding with high
32 remineralised carbon fluxes in this area (station 44; Lemaître et al., 2017) (see section 4.2.2). The largest drawdown in
33 DFe:NO₃⁻ ratios was observed between stations 34 and 38 and was likely due to the intrusion of the IcSPMW, this water mass
34 exhibiting low DFe and high in NO₃⁻ (from 7 to 8 μmol L⁻¹) concentrations. Similarly, the SAIW exhibited high NO₃⁻

1 concentrations. Both the IcSPMW and the SAIW sourced from the NAC. The NAC as it flows along the coast of North
2 America receives atmospheric depositions from anthropogenic sources (Shelley et al., 2017; 2015) which deliver high N
3 relative to Fe (Jickells and Moore, 2015) and might be responsible for the observed ranges.

4 **5 Conclusion**

5 The DFe concentrations measured during this study were in good agreement with previous studies that spanned the West
6 European Basin. However, within the Irminger Basin the DFe concentrations measured during this study were up to 3 times
7 higher than those measured by Rijkenberg et al. (2014) in deep waters (> 1000 m depth). This is likely explained by the
8 different water masses encountered (i.e. the Polar Intermediate Water, ~ 2800 m depth) and by a stronger signal of the Iceland
9 Scotland Overflow Water (ISOW) from 1200 to 2300 m depth. This corresponded to the most striking feature of the whole
10 section with DFe concentrations reaching up to 2.5 nmol L⁻¹ within the ISOW, Denmark Strait Overflow Water (DSOW) and
11 Labrador Sea Water (LSW), three water masses that are part of the Deep Western Boundary Current and was likely the result
12 of a lateral advection of particles in the Irminger. However, as these water masses reached the Labrador Sea, lower DFe levels
13 were measured. These differences could be explained by different processes occurring within the benthic nepheloid layers,
14 where DFe was sometimes trapped onto particles due to Mn-sediment within the Labrador Sea (Gourain et al., 2018) and
15 sometimes released from the sediment potentially as a result of interactions with dissolved organic matter. Such Fe-binding
16 organic ligands could have also been produced locally due to the intense remineralisation rate reported by Lemaître et al.
17 (2017) of biogenic particles (Boyd et al., 2010; Gourain et al., 2018). The LSW exhibited increasing DFe concentrations along
18 its flow path, likely resulting from sediment inputs at the Newfoundland Margin. Although DFe inputs through hydrothermal
19 activity were expected at the slow spreading Reykjanes Ridge (Baker and German, 2004b; German et al., 1994), our data did
20 not provide evidence of this specific source as previously suggested by Achterberg et al. (2018) at ~60°N.
21 In surface waters several sources of DFe were highlighted especially close to land, with riverine inputs from the Tagus River
22 at the Iberian margin (Menzel Barraqueta et al., 2018) and meteoric inputs (including coastal runoff and glacial meltwater) at
23 the Newfoundland and Greenland margins (Benetti et al., 2016). Substantial sediment input was observed at all margins but
24 with varying intensity. The highest DFe sediment input was located at the Newfoundland margin, while the lowest was
25 observed at the eastern Greenland margin. These differences could be explained by the different nature of particles with the
26 most lithogenic located at the Iberian margin and the most biogenic, at the Newfoundland margin (Gourain et al., 2018).
27 Although previous studies (e.g. Jickells et al., 2005; Shelley et al., 2015) reported that atmospheric inputs substantially
28 fertilized surface waters from the West European Basin, in our study, only stations located in the West European and Iceland
29 Basins exhibited enhanced SML DFe inventories with lower TTADs. However, these TTADs were about three times higher
30 than those reported for Saharan dust inputs and thus atmospheric deposition appeared to be a minor source of Fe during the
31 sampling period. Finally, there was evidence of convective inputs of the LSW to surface seawater caused by long tip jet event

1 (Piron et al., 2016) that deepened the winter mixed layer down to ~ 1200 m depth (Zunino et al., 2017), in which Fe was in
2 excess of nitrate and therefore, Fe was not limiting.

3 **Acknowledgements**

4 We are greatly indebted to the master, Gilles Ferrand, the officers and crew from the N/O *Pourquoi Pas?* for their logistic
5 support during the GEOVIDE voyage. We would like to give a special thanks to Pierre Branellec, Michel Hamon, Catherine
6 Kermabon, Philippe Le Bot, Stéphane Leizour, Olivier Ménage (Laboratoire d'Océanographie Physique et Spatiale), Fabien
7 Pérault and Emmanuel de Saint Léger (Division Technique de l'INSU, Plouzané, France) for their technical expertise during
8 clean CTD deployments as well as Emilie Grosteffan and Manon Le Goff for the analysis of nutrients. We also wanted to
9 thank the Pôle Spectrométrie Océan (PSO, Plouzané, France) for letting us use the Element XR HR-ICP-MS. Greg Cutter is
10 also strongly acknowledged for his help in setting up the new French clean sampling system. Catherine Schmechtig is thanked
11 for the LEFE-CYBER database management. This work was funded by the French National Research Agency ANR
12 GEOVIDE (ANR-13-BS06-0014) and RPDOc BITMAP (ANR-12-PDOC-0025-01), the French National Center for
13 Scientific Research (CNRS-LEFE-CYBER), the LabexMER (ANR-10-LABX-19) and Ifremer and was supported for the
14 logistic by DT-INSU and GENAVIR. Manon Tonnard was supported by a cotutelle joint PhD scholarship from the Université
15 de Bretagne Occidentale (UBO-IUEM) and the University of Tasmania (UTAS-IMAS).

16

17 All dissolved iron (DFe) data are available in the supplementary material S1.

18

19 **References**

20 Achterberg, E. P., Steigenberger, S., Marsay, C. M., LeMoigne, F. A., Painter, S. C., Baker, A. R., Connelly, D. P.,
21 Moore, C. M., Tagliabue, A., and Tanhua, T.: Iron Biogeochemistry in the High Latitude North Atlantic Ocean, Scientific
22 reports, 8, 1-15, 10.1038/s41598-018-19472-1, 2018.

23 Aminot, A., and Kerouel, R.: Dosage automatique des nutriments dans les eaux marines, Quae ed., 2007.

24 Annett, A. L., Skiba, M., Henley, S. F., Venables, H. J., Meredith, M. P., Statham, P. J., and Ganeshram, R. S.:
25 Comparative roles of upwelling and glacial iron sources in Ryder Bay, coastal western Antarctic Peninsula, Marine
26 Chemistry, 176, 21-33, 10.1016/j.marchem.2015.06.017, 2015.

27 Bacon, S., Gould, W. J., and Jia, Y.: Open-ocean convection in the Irminger Sea, Geophysical Research Letters, 30,
28 1246, doi:10.1029/2002GL016271, 2003.

29 Baker, A. R., Adams, C., Bell, T. G., Jickells, T. D., and Ganzeveld, L.: Estimation of atmospheric nutrient inputs
30 to the Atlantic Ocean from 50°N to 50°S based on large-scale field sampling: Iron and other dust-associated elements,
31 Global Biogeochemical Cycles, 27, 755-767, 10.1002/gbc.20062, 2013.

- 1 Baker, A. T., and German, C. R.: On the Global Distribution of Hydrothermal vent Fields, in: Mid-Ocean Ridges,
2 edited by: German, C. R., Lin, J., and Parson, L. M., 2004a.
- 3 Baker, E. T., and German, C. R.: Hydrothermal Interactions Between the Lithosphere and Oceans, in: Mid-Ocean
4 Ridges, edited by: German, C. R., Lin, J., and Parson, L. M., Geophysical Monograph Series, AGU, 245-266, 2004b.
- 5 Barton, A. D., Greene, C. H., Monger, B. C., and Pershing, A. J.: The Continuous Plankton Recorder survey and the
6 North Atlantic Oscillation: Interannual- to Multidecadal-scale patterns of phytoplankton variability in the North Atlantic
7 Ocean, *Progress in Oceanography*, 58, 337-358, 10.1016/j.pocean.2003.08.012, 2003.
- 8 Batchelli, S., Muller, F. L. L., Chang, K. C., and Lee, C. L.: Evidence for Strong but Dynamic Iron-Humic
9 Colloidal Associations in Humic-Rich Coastal Waters., *Environmental Science & Technology*, 44, 8485-8490, 2010.
- 10 Benetti, M., Reverdin, G., Pierre, C., Khatiwala, S., Tournadre, B., Olafsdottir, S., and Naamar, A.: Variability of
11 sea ice melt and meteoric water input in the surface Labrador Current off Newfoundland, *Journal of Geophysical Research*
12 *Oceans*, 121, 2841-2855, doi:10.1002/2015JC011302., 2016.
- 13 Benetti, M., Reverdin, G., Lique, C., Yashayaev, I., Holliday, N. P., Tynan, E., Torres-Valdes, S., Lherminier, P.,
14 Tréguer, P., and Sarthou, G.: Composition of freshwater in the spring of 2014 on the southern Labrador shelf and slope,
15 *Journal of Geophysical Research: Oceans*, 122, 1102-1121, 10.1002/2016jc012244, 2017.
- 16 Bersch, M., Yashayaev, I., and Koltermann, K. P.: Recent changes of the thermohaline circulation in the subpolar
17 North Atlantic, *Ocean Dynamics*, 57, 223-235, 10.1007/s10236-007-0104-7, 2007.
- 18 Bhatia, M. P., Kujawinski, E. B., Das, S. B., Breier, C. F., Henderson, P. B., and Charette, M. A.: Greenland
19 meltwater as a significant and potentially bioavailable source of iron to the ocean, *Nature Geoscience*, 2013, 274-278,
20 10.1038/ngeo1746, 2013.
- 21 Bonnet, S., and Guieu, C.: Dissolution of atmospheric iron in seawater, *Geophysical Research Letters*, 31,
22 10.1029/2003gl018423, 2004.
- 23 Bonnet, S., and Guieu, C.: Atmospheric forcing on the annual iron cycle in the western Mediterranean Sea: A 1-
24 year survey, *Journal of Geophysical Research*, 111, 10.1029/2005jc003213, 2006.
- 25 Boyd, P. W., Watson, A. J., Law, C. S., Abraham, E. R., Trull, T., Murdoch, R., Bakker, D. C. E., Bowie, A. R.,
26 Buesseler, K. O., Chang, H., Charette, M., Croot, P., Downing, K., Frew, R., Gall, M., Hadfield, M., Hall, J., Harvey, M.,
27 Jameson, G., LaRoche, J., Liddicoat, M., Ling, R., Maldonado, M. T., McKay, R. M., Nodder, S., Pickmere, S., Pridmore,
28 R., Rintoul, S., Safi, K., Sutton, P., Strzepek, R., Tanneberger, K., Turner, S., Waite, A., and Zeldis, J.: A mesoscale
29 phytoplankton bloom in the polar Southern Ocean stimulated by iron fertilization, *Nature*, 407, 695-702, 2000.
- 30 Boyd, P. W., and Ellwood, M. J.: The biogeochemical cycle of iron in the ocean, *Nature Geoscience*, 3, 675-682,
31 10.1038/ngeo964, 2010.
- 32 Boyd, P. W., Ibanami, E., Sander, S. G., Hunter, K. A., and Jackson, G. A.: Remineralization of upper ocean
33 particles: Implications for iron biogeochemistry, *Limnology and Oceanography*, 55, 1271-1288, 10.4319/lo.2010.55.3.1271,
34 2010.
- 35 Buck, C. S., Landing, W. M., Resing, J. A., and Measures, C. I.: The solubility and deposition of aerosol Fe and
36 other trace elements in the North Atlantic Ocean: Observations from the A16N CLIVAR/CO2 repeat hydrography section,
37 *Marine Chemistry*, 120, 57-70, 10.1016/j.marchem.2008.08.003, 2010.

- 1 Canário, J., Vale, C., Caetano, M., and Madureira, M. J.: Mercury in contaminated sediments and pore waters
2 enriched in sulphate (Tagus Estuary, Portugal), *Environmental Pollution*, 126, 425-433, 10.1016/S0269-7491(03)00234-3,
3 2003.
- 4 Charette, M. A., Morris, P. J., Henderson, P. B., and Moore, W. S.: Radium isotope distributions during the US
5 GEOTRACES North Atlantic cruises, *Marine Chemistry*, 177, 184-195, 10.1016/j.marchem.2015.01.001, 2015.
- 6 Chen, Y. J.: Influence of the Iceland mantle plume on crustal accretion at the inflated Reykjanes Ridge: Magma lens
7 and low hydrothermal activity, *Journal of Geophysical Research*, 108, 2524, 2003.
- 8 Chester, R., Murphy, K. J. T., Lin, F. J., Berry, A. S., Bradshaw, G. A., and Corcoran, P. A.: Factors controlling the
9 solubilities of trace-metals from nonremote aerosols deposited to the sea-surface by the dry deposition mode, *Marine*
10 *Chemistry*, 42, 107-126, 10.1016/0304-4203(93)90241-f, 1993.
- 11 Conway, T. M., and John, S. G.: Quantification of dissolved iron sources to the North Atlantic Ocean, *Nature*, 511,
12 212-215, 10.1038/nature13482, 2014.
- 13 Cooper, L. W., Whitley, T. E., Grebmeier, J. M., and Weingartner, T.: The nutrient, salinity, and stable oxygen
14 isotope composition of Bering and Chukchi Seas waters in and near the Bering Strait, *Journal of Geophysical Research*, 102,
15 12,563-512,573, 1997.
- 16 Cooper, L. W., McClelland, J. W., Holmes, R. M., Raymond, P. A., Gibson, J. J., Guay, C. K., and Peterson, B. J.:
17 Flow-weighted values of runoff tracers ($\delta^{18}\text{O}$, DOC, Ba, alkalinity) from the six largest Arctic rivers, *Geophysical Research*
18 *Letters*, 35, 1-5, 10.1029/2008GL035007, 2008.
- 19 Crane, K., Johnson, L., Appelgate, B., Nishimura, C., Buck, R., Jones, C., Vogt, P., and Kos'yan, R.: Volcanic and
20 Seismic Swarm Events on the Reykjanes Ridge and Their Similarities to Events on Iceland: Results of a Rapid Response
21 Mission, *Marine Geophysical Researches*, 19, 319-338, 1997.
- 22 Cutter, G., Casciotti, K., Croot, P., Geibert, W., Heimburger, L. E., Lohan, M., Planquette, H., and van de Flierdt,
23 T.: Sampling and the Sample-handling Protocols for GEOTRACES Cruises, 2017.
- 24 Daniault, N., Mercier, H., Lherminier, P., Sarafanov, A., Falina, A., Zunino, P., Pérez, F. F., Ríos, A. F., Ferron, B.,
25 Huck, T., Thierry, V., and Gladyshev, S.: The northern North Atlantic Ocean mean circulation in the early 21st century,
26 *Progress in Oceanography*, 146, 142-158, 10.1016/j.pocean.2016.06.007, 2016.
- 27 de Barros, M. C.: A case study of waste inputs in the Tagus estuary, in: *The role of the Oceans as a Waste Disposal*
28 *Option*, edited by: Kullenberg, G., NATO ASI Series; Series C: Mathematical and Physical Sciences, 172, Springer
29 Netherlands, 307-324, 1986.
- 30 de Jong, M. F., van Aken, H. M., Våge, K., and Pickart, R. S.: Convective mixing in the central Irminger Sea:
31 2002–2010, *Deep Sea Research Part I: Oceanographic Research Papers*, 63, 36-51, 10.1016/j.dsr.2012.01.003, 2012.
- 32 Dehairs, F., Shopova, D., Ober, S., Veth, C., and Goeyens, L.: Particulate barium stocks and oxygen consumption
33 in the Southern Ocean mesopelagic water column during spring and early summer: Relationship with export production,
34 *Deep Sea Research II*, 44, 497-516, 10.1016/S0967-0645(96)00072-0, 1997.
- 35 Deng, F., Henderson, G. M., Castrillejo, M., and Perez, F. F.: Evolution of ^{231}Pa and ^{230}Th in overflow waters of
36 the North Atlantic, *Biogeosciences*, 1-24, 10.5194/bg-2018-191, 2018.

- 1 Fagel, N., Robert, C., and Hilaire-Marcel, C.: Clay mineral signature of the NW Atlantic Boundary Undercurrent,
2 *Marine Geology*, 130, 19-28, 1996.
- 3 Fagel, N., Robert, C., Preda, M., and Thorez, J.: Smectite composition as a tracer of deep circulation: the case of the
4 Northern North Atlantic, *Marine Geology*, 172, 309-330, 2001.
- 5 Ferron, B., Kokoszka, F., Mercier, H., Lherminier, P., Huck, T., Rios, A., and Thierry, V.: Variability of the
6 Turbulent Kinetic Energy Dissipation along the A25 Greenland–Portugal Transect Repeated from 2002 to 2012, *Journal of*
7 *Physical Oceanography*, 46, 1989-2003, 10.1175/jpo-d-15-0186.1, 2016.
- 8 Figueres, G., Martin, J. M., Meybeck, M., and Seyler, P.: A comparative study of mercury contamination in the
9 Tagus estuary (Portugal) and major French estuaries (Gironde, Loire, Rhone), *Estuarine, Coastal and Shelf Science*, 20, 183-
10 203, 1985.
- 11 Fiuza, A.: Hidrologia e dinamica das aguas costeiras de Portugal, Ph. D., Universidade de Lisboa, Lisboa, Portugal,
12 unpublished, 1984.
- 13 Follows, M., and Dutkiewicz, S.: Meteorological modulation of the North Atlantic Spring Bloom, *Deep Sea*
14 *Research Part II: Topical Studies in Oceanography*, 49, 321-344, 2001.
- 15 García-Ibáñez, M. I., Pardo, P. C., Carracedo, L. I., Mercier, H., Lherminier, P., Ríos, A. F., and Pérez, F. F.:
16 Structure, transports and transformations of the water masses in the Atlantic Subpolar Gyre, *Progress in Oceanography*, 135,
17 18-36, 10.1016/j.pocean.2015.03.009, 2015.
- 18 García-Ibáñez, M. I., Pérez, F. F., Lherminier, P., Zunino, P., Mercier, H., and Tréguer, P.: Water mass distributions
19 and transports for the 2014 GEOVIDE cruise in the North Atlantic, *Biogeosciences*, 15, 2075-2090, 10.5194/bg-15-2075-
20 2018, 2018.
- 21 García-Ibáñez, M. I., Pérez, F. F., Lherminier, P., Zunino, P., and Tréguer, P.: Water mass distributions and
22 transports for the 2014 GEOVIDE cruise in the North Atlantic, *Biogeosciences*, this issue.
- 23 Gaudencio, M. J., Guerra, M. T., and Glemarec, M.: Recherches biosédimentaires sur la zone maritime de l'estuaire
24 du Tage, Portugal: données sédimentaires préliminaires. , in: *Estuaries and Coasts: Spatial and Temporal Intercomparisons*,
25 edited by: Elliot, M., and Ducrotot, J. C., Olsen and Olsen, Fredensborg, 11-16, 1991.
- 26 German, C. R., Briem, J., Chin, C. S., Danielsen, M., Holland, S., James, R. H., Jonsdottir, A., Ludford, E., Moser,
27 C., Olafsson, J., Palmer, M. R., and Rudnicki, M. D.: Hydrothermal activity on the Reykjanes Ridge: the Steinahóll vent-
28 field at 63°06'N, *Earth and Planetary Science Letters*, 121, 647-654, 1994.
- 29 Gerringa, L. J. A., Blain, S., Laan, P., Sarthou, G., Veldhuis, M. J. W., Brussaard, C. P. D., Viollier, E., and
30 Timmermans, K. R.: Fe-binding dissolved organic ligands near the Kerguelen Archipelago in the Southern Ocean (Indian
31 sector), *Deep Sea Research Part II: Topical Studies in Oceanography*, 55, 606-621, 10.1016/j.dsr2.2007.12.007, 2008.
- 32 Gerringa, L. J. A., Slagter, H. A., Bown, J., van Haren, H., Laan, P., de Baar, H. J. W., and Rijkenberg, M. J. A.:
33 Dissolved Fe and Fe-binding organic ligands in the Mediterranean Sea – GEOTRACES G04, *Marine Chemistry*, 194, 100-
34 113, 10.1016/j.marchem.2017.05.012, 2017.
- 35 Gourain, A., Planquette, H., Cheize, M., Menzel-Barraqueta, J. L., Boutorh, J., Shelley, R. U., Pereira-Contreira, L.,
36 Lemaitre, N., Lacan, F., Lherminier, P., and Sarthou, G.: particulate trace metals along the GEOVIDE section,
37 *Biogeosciences*, 2018.

- 1 Guerzoni, S., Chester, R., Dulac, F., Herut, B., Loye-Pilot, M.-D., Measures, C., Migon, C., Molinaroli, E., Moulin,
2 C., Rossini, P., Saydam, C., Soudine, A., and Ziveri, P.: The role of atmospheric deposition in the biogeochemistry of the
3 Mediterranean Sea, *Progress in Oceanography*, 44, 147-190, 1999.
- 4 Guieu, C., Loye-Pilot, M. D., Benyahya, L., and Dufour, A.: Spatial variability of atmospheric fluxes of metals (Al,
5 Fe, Cd, Zn and Pb) and phosphorus over the whole Mediterranean from a one-year monitoring experiment: Biogeochemical
6 implications, *Marine Chemistry*, 120, 164-178, 10.1016/j.marchem.2009.02.004, 2010.
- 7 Guieu, C., Aumont, O., Paytan, A., Bopp, L., Law, C. S., Mahowald, N., Achterberg, E. P., Marañón, E., Salihoglu,
8 B., Crise, A., Wagener, T., Herut, B., Desboeufs, K., Kanakidou, M., Olgun, N., Peters, F., Pulido-Villena, E., Tovar-
9 Sanchez, A., and Völker, C.: The significance of the episodic nature of atmospheric deposition to Low Nutrient Low
10 Chlorophyll regions, *Global Biogeochemical Cycles*, 28, 1179-1198, 10.1002/2014gb004852, 2014.
- 11 Harrison, W. G., Yngve Børsheim, K., Li, W. K. W., Maillet, G. L., Pepin, P., Sakshaug, E., Skogen, M. D., and
12 Yeats, P. A.: Phytoplankton production and growth regulation in the Subarctic North Atlantic: A comparative study of the
13 Labrador Sea-Labrador/Newfoundland shelves and Barents/Norwegian/Greenland seas and shelves, *Progress in*
14 *Oceanography*, 114, 26-45, 10.1016/j.pocean.2013.05.003, 2013.
- 15 Hatta, M., Measures, C. I., Wu, J., Roshan, S., Fitzsimmons, J. N., Sedwick, P., and Morton, P.: An overview of
16 dissolved Fe and Mn distributions during the 2010-2011 US GEOTRACES north Atlantic cruises: GEOTRACES GA03,
17 *Deep-Sea Research Part II-Topical Studies in Oceanography*, 116, 117-129, 10.1016/j.dsr2.2014.07.005, 2015.
- 18 Hawkings, J. R., Wadham, J. L., Tranter, M., Raiswell, R., Benning, L. G., Statham, P. J., Tedstone, A., Nienow, P.,
19 Lee, K., and Telling, J.: Ice sheets as a significant source of highly reactive nanoparticulate iron to the oceans, *Nature*
20 *communications*, 5, 1-8, 10.1038/ncomms4929, 2014.
- 21 Henson, S. A., Dunne, J. P., and Sarmiento, J. L.: Decadal variability in North Atlantic phytoplankton blooms,
22 *Journal of Geophysical Research*, 114, 10.1029/2008jc005139, 2009.
- 23 Ho, T.-Y., Quigg, A., Finkel, Z. V., Milligan, A. J., Wyman, K., Falkowski, P. G., and Morel, F. M. M.: The
24 elemental composition of some marine phytoplankton, *Journal of Phycology*, 39, 1145-1159, 2003.
- 25 Homoky, W. B., Hembury, D. J., Hepburn, L. E., Mills, R. A., Statham, P. J., Fones, G. R., and Palmer, M. R.: Iron
26 and manganese diagenesis in deep sea volcanogenic sediments and the origins of pore water colloids, *Geochimica Et*
27 *Cosmochimica Acta*, 75, 5032-5048, 10.1016/j.gca.2011.06.019, 2011.
- 28 Homoky, W. B., John, S. G., Conway, T. M., and Mills, R. A.: Distinct iron isotopic signatures and supply from
29 marine sediment dissolution, *Nature Communications*, 4, 10.1038/ncomms3143, 2013.
- 30 Humphreys, M. P., Griffiths, A. M., Achterberg, E. P., Holliday, N. P., Rérolle, V., Menzel Barraqueta, J. L.,
31 Couldrey, M. P., Oliver, K. I., Hartman, S. E., and Esposito, M.: Multidecadal accumulation of anthropogenic and
32 remineralized dissolved inorganic carbon along the Extended Ellett Line in the northeast Atlantic Ocean, *Global*
33 *Biogeochemical Cycles*, 30, 293-310, doi: 10.1002/2015GB005246, 2016.
- 34 Hunke, E. C., Notz, D., Turner, A. K., and Vancoppenolle, M.: The multiphase physics of sea ice: a review for
35 model developers, *The Cryosphere*, 5, 989-1009, 10.5194/tc-5-989-2011, 2011.
- 36 Janssens, J., Meiners, K. M., Tison, J.-L., Dieckmann, G., Delille, B., and Lannuzel, D.: Incorporation of iron and
37 organic matter into young Antarctic sea ice during its initial growth stages, *Elementa: Science of the Anthropocene*, 4,
38 000123, 10.12952/journal.elementa.000123, 2016.

- 1 Jickells, T., and Moore, C. M.: The importance of atmospheric deposition for ocean productivity, *Annual Review of*
2 *Ecology, Evolution, and Systematics*, 46, 481-501, 10.1146/annurev-ecolsys-112414-054118, 2015.
- 3 Jickells, T. D., An, Z. C., Andersen, K. K., Baker, A. R., Bergametti, G., Brooks, N., Cao, J. J., Boyd, P. W., Duce,
4 R. A., Hunter, K. A., Kawahata, H., Kubilay, N., laRoche, J., Liss, P. S., Mahowald, N., Prospero, J. M., Ridgwell, A. J.,
5 Tegen, I., and Torres, R.: Global iron connections between desert dust, ocean biogeochemistry, and climate, *Science*, 308,
6 67-71, 2005.
- 7 Jones, E. P., Anderson, L. G., and Swift, J. H.: Distribution of ATLantic and Pacific waters in the upper Arctic
8 Ocean: Implications for circulation, *Geophysical Research Letters*, 25, 765-768, 1998.
- 9 Kan, C. C., Chen, W. H., Wan, M. W., Phatai, P., Wittayakun, J., and Li, K. F.: The preliminary study of iron and
10 manganese removal from groundwater by NaOCl oxidation and MF filtration, *Sustain. Environ. Res.*, 22, 25-30, 2012.
- 11 Kara, A. B., Rochford, P. A., and Hurlburt, H. E.: An optimal definition for ocean mixed layer depth, *Journal of*
12 *Geophysical Research*, 105, 16,803-816,821, 10.1029/2000JC900072, 2000.
- 13 Kissel, C., Laj, C., Mulder, T., Wandres, C., and Cremer, M.: The magnetic fraction: A tracer of deep water
14 circulation in the North Atlantic, *Earth and Planetary Science Letters*, 288, 444-454, 10.1016/j.epsl.2009.10.005, 2009.
- 15 Klunder, M. B., Bauch, D., Laan, P., de Baar, H. J. W., van Heuven, S. M. A. C., and Ober, S.: Dissolved iron in
16 the Arctic shelf seas and surface waters of the Central Arctic Ocean: impact of Arctic river water and ice-melt, *Journal of*
17 *Geophysical Research*, 117, 1-18, 2012.
- 18 Lackschewitz, K. S., Endler, R., Gehrke, B., Wallrabe-Adams, H.-J., and Thiede, J.: Evidence for topography- and
19 current-controlled deposition on the reykjanes Ridge between 59°N and 60°N, *Deep-Sea Research I*, 43, 1683-1711, 1996.
- 20 Laes, A., Blain, S., Laan, P., Achterberg, E. P., Sarthou, G., and de Baar, H. J. W.: Deep dissolved iron profiles in
21 the eastern North Atlantic in relation to water masses, *Geophysical Research Letters*, 30, 10.1029/2003gl017902, 2003.
- 22 Lagerström, M. E., Field, M. P., Seguret, M., Fischer, L., Hann, S., and Sherrell, R. M.: Automated on-line flow-
23 injection ICP-MS determination of trace metals (Mn, Fe, Co, Ni, Cu and Zn) in open ocean seawater: Application to the
24 GEOTRACES program, *Marine Chemistry*, 155, 71-80, 10.1016/j.marchem.2013.06.001, 2013.
- 25 Lambelet, M., van de Flierdt, T., Crocket, K., Rehkamper, M., Katharina, K., Coles, B., Rijkenberg, M. J. A.,
26 Gerringa, L. J. A., de Baar, H. J. W., and Steinfeldt, R.: Neodymium isotopic composition and concentration in the western
27 North Atlantic Ocean: Results from the GEOTRACES GA02 section, *Geochimica Et Cosmochimica Acta*, 177, 1-29, 2016.
- 28 Le Roy, E., Sanial, V., Charette, M. A., van Beek, P., Lacan, F., Jacquet, S. H. M., Henderson, P. B., Souhaut, M.,
29 García-Ibáñez, M. I., Jeandel, C., Pérez, F. F., and Sarthou, G.: The 226Ra–Ba relationship in the North Atlantic during
30 GEOTRACES-GA01, *Biogeosciences*, 15, 3027-3048, 10.5194/bg-15-3027-2018, 2018.
- 31 Lemaitre, N., Planchon, F., Planquette, H., Dehairs, F., Fonseca-Batista, D., Roukaerts, A., Deman, F., Tang, Y.,
32 Mariez, C., and Sarthou, G.: High variability of export fluxes along the North Atlantic GEOTRACES section GA01:
33 Particulate organic carbon export deduced from the 234Th method *Biogeosciences*, 1-38, 10.5194/bg-2018-190, 2018.
- 34 Lemaitre, N., planquette, H., Planchon, F., Sarthou, G., Jacquet, S., Garcia-Ibanez, M. I., Gourain, A., Cheize, M.,
35 Monin, L., Andre, L., Laha, P., Terryn, H., and Dehairs, F.: Particulate barium tracing significant mesopelagic carbon
36 remineralisation in the North Atlantic *Biogeosciences Discussions*, 2017.

- 1 Lohan, M. C., and Bruland, K. W.: Elevated Fe(II) and Dissolved Fe in Hypoxic Shelf Waters off Oregon and
2 Washington: An Enhanced Source of Iron to Coastal Upwelling Regimes, *Environmental Science & Technology*, 42, 6462-
3 6468, 10.1021/es800144j, 2008.
- 4 Longhurst, A. R.: *Ecological geography of the Sea*, Second Edition ed., Elsevier Academic Press publications,
5 Burlington, 542 pp., 2007.
- 6 Louanchi, F., and Najjar, R. G.: Annual cycles of nutrients and oxygen in the upper layers of the North Atlantic
7 Ocean, *Deep Sea Research Part II: Topical Studies in Oceanography*, 48, 2155-2171, 2001.
- 8 Markus, T., Stroeve, J. C., and Miller, J.: Recent changes in Arctic sea ice melt onset, freezeup, and melt season
9 length, *Journal of Geophysical Research*, 114, 10.1029/2009jc005436, 2009.
- 10 Marshall, J., and Schott, F.: Open-ocean convection: observations, theory, and models, *Reviews of Geophysics*, 37,
11 1-64, doi: 10.1029/98RG02739, 1999.
- 12 Martin, J.-M., Elbaz-Poulichet, F., Guieu, C., Loÿe-Pilot, M.-D., and Han, G.: River versus atmospheric input of
13 material to the Mediterranean Sea: an overview*, *Marine Chemistry*, 28, 159-182, 1989.
- 14 Martin, J. D., and Fitzwater, S. E.: Iron deficiency limits phytoplankton growth in the north-east Pacific subarctic,
15 *Nature*, 331, 341-343, 1988.
- 16 Martin, J. H., Fitzwater, S. E., and Gordon, R. M.: Iron deficiencies limits phytoplankton growth in Antarctic
17 waters, *Global Biogeochemical Cycles*, 4, 5-12, 1990.
- 18 Martin, J. H., Coale, K. H., Johnson, K. S., Fitzwater, S. E., Gordon, R. M., Tanner, S. J., Hunter, C. N., Elrod, V.
19 A., Nowicki, J. L., Coley, T. L., Barber, R. T., Lindley, S., Watson, A. J., Van Scoy, K., Law, C. S., Liddicoat, M. I., Ling,
20 R., Stanton, T., Stockel, J., Collins, C., Anderson, A., Bidigare, R., Ondrusek, M., Latasa, M., Millero, F. J., Lee, K., Yao,
21 W., Zhang, J. Z., Friederich, G., Sakamoto, C., Chavez, F., Buck, K., Kolber, Z., Greene, R., Falkowski, P., Chisholm, S.
22 W., Hoge, F., Swift, R., Yungel, J., Turner, S., Nightingale, P., Hatton, A., Liss, P., and Tindale, N. W.: Testing the Iron
23 Hypothesis in Ecosystems of the Equatorial Pacific Ocean, *Nature*, 371, 123-129, 10.1038/371123a0, 1994.
- 24 Measures, C. I., Brown, M. T., Selph, K. E., Apprill, A., Zhou, M., Hatta, M., and Hiscock, W. T.: The influence of
25 shelf processes in delivering dissolved iron to the HNLC waters of the Drake Passage, Antarctica, *Deep Sea Research Part*
26 *II: Topical Studies in Oceanography*, 90, 77-88, 10.1016/j.dsr2.2012.11.004, 2013.
- 27 Melling, H., and Moore, R. M.: Modification of halocline source waters during freezing on the Beaufort Sea shelf:
28 Evidence from oxygen isotopes and dissolved nutrients, *Continental Shelf Research*, 15, 89-113, 1995.
- 29 Menzel Barraqueta, J. L., Schlosser, C., Planquette, H., Gourain, A., Cheize, M., Boutorh, J., Shelley, R. U., Pereira
30 Contreira, L., Gledhill, M., Hopwood, M. J., Lherminier, P., Sarthou, G., and Achterberg, E. P.: Aluminium in the North
31 Atlantic Ocean and the Labrador Sea (GEOTRACES GA01 section): roles of continental inputs and biogenic particle
32 removal, *Biogeosciences Discussions*, 1-28, 10.5194/bg-2018-39, 2018.
- 33 Mercier, H., Lherminier, P., Sarafanov, A., Gaillard, F., Daniault, N., Desbryères, D., Falina, A., Ferron, B.,
34 Gourcuff, C., Huck, T., and Thierry, V.: Variability of the meridional overturning circulation at the Greenland–Portugal
35 OVIDE section from 1993 to 2010, *Progress in Oceanography*, 132, 250-261, 10.1016/j.pocean.2013.11.001, 2015.

- 1 Mil-Homens, M., Branco, V., Lopes, C., Vale, C., Abrantes, F., Boer, W., and Vicente, M.: Using factor analysis to
2 characterise historical trends of trace metal contamination in a sediment core from the Tagus Prodelta, Portugal, *Water, Air,
3 and Soil Pollution*, 197, 277-287, 2009.
- 4 Moore, C. M., Mills, M. M., Langlois, R., Milne, A., Achterberg, E. P., La Roche, J., and Geider, R. J.: Relative
5 influence of nitrogen and phosphorus availability on phytoplankton physiology and productivity in the oligotrophic sub-
6 tropical North Atlantic Ocean, *Limnology and Oceanography*, 53, 291-205, 2008.
- 7 Moore, C. M., Mills, M. M., Arrigo, K. R., Berman-Frank, I., Bopp, L., Boyd, P. W., Galbraith, E. D., Geider, R. J.,
8 Guieu, C., Jaccard, S. L., Jickells, T. D., La Roche, J., Lenton, T. M., Mahowald, N. M., Marañón, E., Marinov, I., Moore, J.
9 K., Nakatsuka, T., Oschlies, A., Saito, M. A., Thingstad, T. F., Tsuda, A., and Ulloa, O.: Processes and patterns of oceanic
10 nutrient limitation, *Nature Geoscience*, 6, 701-710, 10.1038/ngeo1765, 2013.
- 11 Moore, G. W. K.: Gale force winds over the Irminger Sea to the east of Cape Farewell, Greenland, *Geophysical
12 Research Letters*, 30, n/a-n/a, 10.1029/2003gl018012, 2003.
- 13 Nielsdóttir, M. C., Moore, C. M., Sanders, R., Hinz, D. J., and Achterberg, E. P.: Iron limitation of the postbloom
14 phytoplankton communities in the Iceland Basin, *Global Biogeochemical Cycles*, 23, n/a-n/a, 10.1029/2008gb003410, 2009.
- 15 Olafsson, J., Thors, K., and Cann, J. R.: A sudden cruise off Iceland, *RIDGE Events*, 2, 35-28, 1991.
- 16 Oschlies, A.: Nutrient supply to the surface waters of the North Atlantic: A model study, *Journal of Geophysical
17 Research*, 107, 10.1029/2000jc000275, 2002.
- 18 Painter, S. C., Henson, S. A., Forryan, A., Steigenberger, S., Klar, J., Stinchcombe, M. C., Rogan, N., Baker, A. R.,
19 Achterberg, E. P., and Moore, C. M.: An assessment of the vertical diffusive flux of iron and other nutrients to the surface
20 waters of the subpolar North Atlantic Ocean, *Biogeosciences*, 11, 2113-2130, 10.5194/bg-11-2113-2014, 2014.
- 21 Palmer, M. R., Ludford, E. M., German, C. R., and Lilley, M. D.: Dissolved methane and hydrogen in the
22 Steinahóll hydrothermal plume, 63°N, Reykjanes Ridge, in: *Hydrothermal Vents and Processes*, edited by: Parson, L. M.,
23 Walker, C. L., and Dixon, D. R., Special Publications, Geological Society, London, 111-120, 1995.
- 24 Parekh, P., Follows, M. J., and Boyle, E. A.: Decoupling of iron and phosphate in the global ocean, *Global
25 Biogeochemical Cycle*, 19, 2005.
- 26 Parra, M., Delmont, P., Ferragne, A., Latouche, C., Pons, J. C., and Puechmaille, C.: Origin and evolution of
27 smectites in recent marine sediments of the NE Atlantic, *Clay Minerals*, 20, 335-346, 1985.
- 28 Pérez, F. F., Mercier, H., Vázquez-Rodríguez, M., Lherminier, P., Velo, A., Pardo, P. C., Rosón, G., and Ríos, A.
29 F.: Atlantic Ocean CO₂ uptake reduced by weakening of the meridional overturning circulation, *Nature Geoscience*, 6, 146-
30 152, 10.1038/ngeo1680, 2013.
- 31 Pérez, F. F., Treguer, P., Branellec, P., García-Ibáñez, M. I., Lherminier, P., and Sarthou, G.: The 2014 Greenland-
32 Portugal GEOVIDE bottle data (GO-SHIP A25 and GEOTRACES GA01). SEANOE (Ed.), 2018.
- 33 Petrich, C., and Eicken, H.: Growth, structure and properties of sea ice, in: *Sea Ice*. 2nd ed., edited by: Thomas, D.
34 N., and Dieckmann, G. S., Wiley-Blackwell, Oxford, U.K., 23-77, 2010.
- 35 Pickart, R. S., Straneo, F., and Moore, G. W. K.: Is Labrador Sea Water formed in the Irminger basin?, *Deep Sea
36 Research Part I*, 50, 23-52, 2003.

- 1 Piron, A., Thierry, V., Mercier, H., and Caniaux, G.: Argo float observations of basin-scale deep convection in the
2 Irminger sea during winter 2011–2012, *Deep Sea Research Part I: Oceanographic Research Papers*, 109, 76-90,
3 10.1016/j.dsr.2015.12.012, 2016.
- 4 Radic, A., Lacan, F., and Murray, J. W.: Iron isotopes in the seawater of the equatorial Pacific Ocean: New
5 constraints for the oceanic iron cycle, *Earth and Planetary Science Letters*, 306, 1-10, 10.1016/j.epsl.2011.03.015, 2011.
- 6 Ras, J., Claustre, H., and Uitz, J.: Spatial variability of phytoplankton pigment distribution in the Subtropical South
7 Pacific Ocean: comparison between *in situ* and predicted data, *Biogeosciences*, 5, 353-369, 2008.
- 8 Riebesell, U., Schloss, I., and Smetacek, V.: Aggregation of algae released from melting sea ice: implications for
9 seeding and sedimentation, *Polar Biology*, 11, 239-248, 1991.
- 10 Rijkenberg, M. J., Middag, R., Laan, P., Gerringa, L. J., van Aken, H. M., Schoemann, V., de Jong, J. T., and de
11 Baar, H. J.: The distribution of dissolved iron in the West Atlantic Ocean, *PLoS One*, 9, e101323,
12 10.1371/journal.pone.0101323, 2014.
- 13 Sabine, C. L., Feely, R. A., Gruber, N., Key, R. M., Lee, K., Bullister, J. L., Wanninkhof, R., Wong, C. S., Wallace,
14 D. W. R., Tilbrook, B., Millero, F. J., Peng, T.-H., Kozyr, A., Ono, T., and Rios, A. F.: The Oceanic sink for anthropogenic
15 CO₂, *Science*, 305, 367-371, 2004.
- 16 Sanders, R., Brown, L., Henson, S., and Lucas, M.: New production in the Irminger Basin during 2002, *Journal of*
17 *Marine Systems*, 55, 291-310, [http:// dx.doi.org/10.1016/j.jmarsys.2004.09.002](http://dx.doi.org/10.1016/j.jmarsys.2004.09.002), 2005.
- 18 Santos-Echeandia, J., Vale, C., Caetano, M., Pereira, P., and Prego, R.: Effect of tidal flooding on metal distribution
19 in pore waters of marsh sediments and its transport to water column (Tagus estuary, Portugal), *Mar Environ Res*, 70, 358-
20 367, 10.1016/j.marenvres.2010.07.003, 2010.
- 21 Sarthou, G., and Jeandel, C.: Seasonal variations of iron concentrations in the Ligurian Sea and iron budget in the
22 Western Mediterranean Sea, *Marine Chemistry*, 74, 115-129, 10.1016/s0304-4203(00)00119-5, 2001.
- 23 Sarthou, G., Baker, A. R., Kramer, J., Laan, P., Laës, A., Ussher, S., Achterberg, E. P., de Baar, H. J. W.,
24 Timmermans, K. R., and Blain, S.: Influence of atmospheric inputs on the iron distribution in the subtropical North-East
25 Atlantic Ocean, *Marine Chemistry*, 104, 186-202, 10.1016/j.marchem.2006.11.004, 2007.
- 26 Sarthou, G., Vincent, D., Christaki, U., Obernosterer, I., Timmermans, K. R., and Brussaard, C. P. D.: The fate of
27 biogenic iron during a phytoplankton bloom induced by natural fertilisation: Impact of copepod grazing, *Deep Sea Research*
28 *Part II: Topical Studies in Oceanography*, 55, 734-751, 10.1016/j.dsr2.2007.12.033, 2008.
- 29 Sarthou, G., Lherminier, P., Achterberg, E. P., Alonso-Pérez, F., Bucciarelli, E., Boutorh, J., Bouvier, V., Boyle, E.
30 A., Branellec, P., Carracedo, L. I., Casacuberta, N., Castrillejo, M., Cheize, M., Contreira Pereira, L., Cossa, D., Daniault,
31 N., De Saint-Léger, E., Dehairs, F., Deng, F., Desprez de Gésincourt, F., Devesa, J., Foliot, L., Fonseca-Batista, D.,
32 Gallinari, M., García-Ibáñez, M. I., Gourain, A., Grossteffan, E., Hamon, M., Heimbürger, L. E., Henderson, G. M., Jeandel,
33 C., Kermabon, C., Lacan, F., Le Bot, P., Le Goff, M., Le Roy, E., Lefèbvre, A., Leizour, S., Lemaitre, N., Masqué, P.,
34 Ménage, O., Menzel Barraqueta, J.-L., Mercier, H., Perault, F., Pérez, F. F., Planquette, H. F., Planchon, F., Roukaerts, A.,
35 Sanial, V., Sauzède, R., Shelley, R. U., Stewart, G., Sutton, J. N., Tang, Y., Tisnérat-Laborde, N., Tonnard, M., Tréguer, P.,
36 van Beek, P., Zurbrick, C. M., and Zunino, P.: Introduction to the French GEOTRACES North Atlantic Transect (GA01):
37 GEOVIDE cruise, *Biogeosciences Discussions*, 1-24, 10.5194/bg-2018-312, 2018.
- 38 Ocean Data View, <https://odv.awi.de> ODV4, version 4.7.6 (23 March 2016), access: 6 April, 2016.

1 Schroth, A. W., Crusius, J., Hoyer, I., and Campbell, R.: Estuarine removal of glacial iron and implications for iron
2 fluxes to the ocean, *Geophysical Research Letters*, 41, 3951-3958, 10.1002/2014GL060199, 2014.

3 Shelley, R. U., Morton, P. L., and Landing, W. M.: Elemental ratios and enrichment factors in aerosols from the
4 US-GEOTRACES North Atlantic transects, *Deep Sea Research*, 116, 262-272, 2015.

5 Shelley, R. U., Roca-Martí, M., Castrillejo, M., Sanial, V., Masqué, P., Landing, W. M., van Beek, P., Planquette,
6 H., and Sarthou, G.: Quantification of trace element atmospheric deposition fluxes to the Atlantic Ocean (>40°N;
7 GEOVIDE, GEOTRACES GA01) during spring 2014, *Deep Sea Research Part I: Oceanographic Research Papers*, 119, 34-
8 49, 10.1016/j.dsr.2016.11.010, 2017.

9 Shelley, R. U., Landing, W. M., Ussher, S. J., Planquette, H., and Sarthou, G.: Characterisation of aerosol
10 provenance from the fractional solubility of Fe (Al, Ti, Mn, Co, Ni, Cu, Zn, Cd and Pb) in North Atlantic aerosols
11 (GEOTRACES cruises GA01 and GA03) using a two stage leach, *Biogeosciences*, 2018.

12 Shor, A., Lonsdale, P., Hollister, D., and Spencer, D.: Charlie-Gibbs fracture zone: bottom-water transport and its
13 geological effects, *Deep Sea Research*, 27A, 325-345, 1980.

14 Sinha, M. C., Navin, D. A., MacGregor, L. M., Constable, S., Peirce, C., White, A., Heinson, G., and Inglis, M. A.:
15 Evidence for accumulated melt beneath the slow-spreading Mid-Atlantic Ridge, *Philosophical Transactions of the Royal
16 Society A*, 355, 233-253, 1997.

17 Slagter, H. A., Reader, H. E., Rijkenberg, M. J. A., Rutgers van der Loeff, M., de Baar, H. J. W., and Gerringa, L. J.
18 A.: Organic Fe speciation in the Eurasian Basins of the Arctic Ocean and its relation to terrestrial DOM, *Marine Chemistry*,
19 197, 11-25, 10.1016/j.marchem.2017.10.005, 2017.

20 Smallwood, J. R., and White, R. S.: Crustal accretion at the Reykjanes Ridge, 61°-62°N, *Journal of Geophysical
21 Research: Solid Earth*, 103, 5185-5201, 10.1029/97jb03387, 1998.

22 Statham, P. J., Skidmore, M., and Tranter, M.: Inputs of glacially derived dissolved and colloidal iron to the coastal
23 ocean and implications for primary productivity, *Global Biogeochemical Cycles*, 22, 1-11, 10.1029/2007GB003106, 2008.

24 Sunda, W. G., and Huntsman, S. A.: Iron uptake and growth limitation in oceanic and coastal phytoplankton,
25 *Marine Chemistry*, 50, 189-206, 10.1016/0304-4203(95)00035-p, 1995.

26 Sutherland, D. A., Pickart, R. S., Peter Jones, E., Azetsu-Scott, K., Jane Eert, A., and Ólafsson, J.: Freshwater
27 composition of the waters off southeast Greenland and their link to the Arctic Ocean, *Journal of Geophysical Research*, 114,
28 10.1029/2008jc004808, 2009.

29 Tanhua, T., Olsson, K. A., and Jeansson, E.: Formation of Denmark Strait overflow water and its hydro-chemical
30 composition, *Journal of Marine Systems*, 57, 264-288, 10.1016/j.jmarsys.2005.05.003, 2005.

31 Teng, Z., Huang, J. Y., Fujito, K., and Takizawa, S.: Manganese removal by hollow fiber micro-filter. Membrane
32 separation for drinking water, *European Conference on Desalination and the Environment*, Amsterdam, 28 May, 2001.

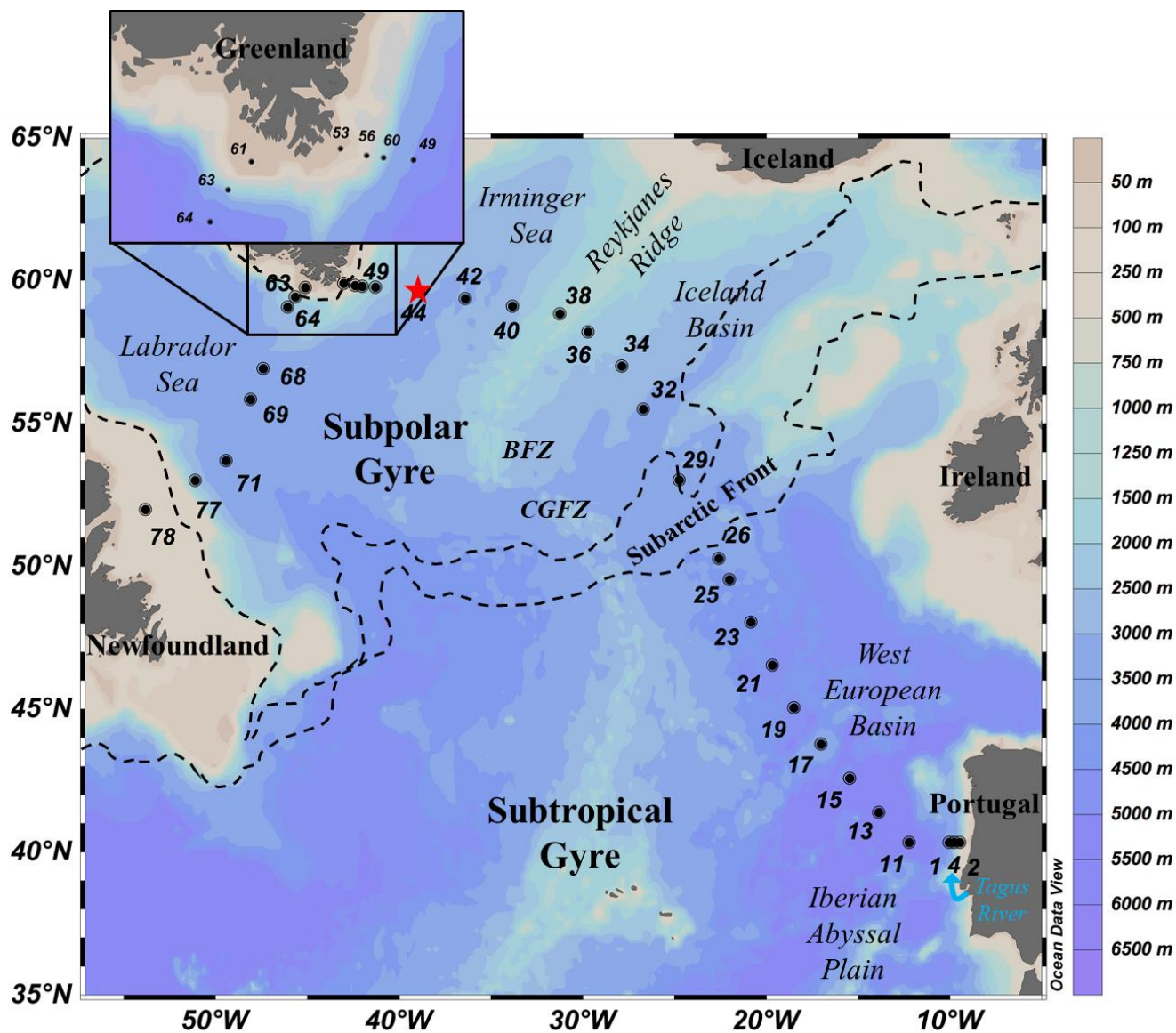
33 Thuróczy, C. E., Gerringa, L. J. A., Klunder, M. B., Middag, R., Laan, P., Timmermans, K. R., and de Baar, H. J.
34 W.: Speciation of Fe in the Eastern North Atlantic Ocean, *Deep Sea Research Part I: Oceanographic Research Papers*, 57,
35 1444-1453, 10.1016/j.dsr.2010.08.004, 2010.

- 1 Tonnard, M., Donval, A., Lampert, L., Tréguer, P., Bowie, A. R., van der Merwe, P., planquette, H., Claustre, H.,
2 Dimier, C., Ras, J., and Sarthou, G.: Phytoplankton assemblages in the North Atlantic Ocean and in the Labrador Sea along
3 the GEOVIDE section (GEOTRACES section GA01) determined by CHEMTAX analysis from HPLC pigment data,
4 Biogeosciences, in prep.
- 5 Tovar-Sanchez, A., Duarte, C. M., Alonso, J. C., Lacorte, S., Tauler, R., and Galban-Malagon, C.: Impacts of
6 metals and nutrients released from melting multiyear Arctic sea ice, *Journal of Geophysical Research-Oceans*, 115,
7 10.1029/2009jc005685, 2010.
- 8 Tréguer, P. J., and De La Rocha, C. L.: The world ocean silica cycle, *Ann Rev Mar Sci*, 5, 477-501,
9 10.1146/annurev-marine-121211-172346, 2013.
- 10 Twining, B. S., Baines, S. B., Fisher, N. S., and Landry, M. R.: Cellular iron contents of plankton during the
11 Southern Ocean Iron Experiment (SOFEX), *Deep Sea Research Part I: Oceanographic Research Papers*, 51, 1827-1850,
12 10.1016/j.dsr.2004.08.007, 2004.
- 13 Van Beusekom, J. E. E.: Distribution of aluminium in surface waters of the North Sea: influence of suspended
14 matter., in: *Biogeochemistry and Distribution of Suspended Matter in the North Sea and Implications to fisheries Biology*,
15 edited by: Kempe, S., Mittleitungen aus dem Geologisch-Paläontologischen Institut der Universität Hamburg,
16 SCOPE/UNEP Sonderband, 117-136, 1988.
- 17 von Appen, W.-J., Koszalka, I. M., Pickart, R. S., Haine, T. W. N., Mastropole, D., Magaldi, M. G., Valdimarsson,
18 H., Girton, J., Jochumsen, K., and Krahnemann, G.: The East Greenland Spill Jet as an important component of the Atlantic
19 Meridional Overturning Circulation, *Deep Sea Research Part I: Oceanographic Research Papers*, 92, 75-84,
20 10.1016/j.dsr.2014.06.002, 2014.
- 21 Wadhams, P.: *Ice in the Ocean*, Gordon and Breach Science Publishers, London, UK, 2000.
- 22 Wagener, T., Guieu, C., and Leblond, N.: Effects of dust deposition on iron cycle in the surface Mediterranean Sea:
23 results from a mesocosm seeding experiment, *Biogeosciences Discussions*, 7, 2799-2830, 2010.
- 24 Woodgate, R. A., and Aagaard, K.: Revising the Bering Strait freshwater flux into the Arctic Ocean, *Geophysical*
25 *Research Letters*, 32, 10.1029/2004GL021747., 2005.
- 26 Wuttig, K., Wagener, T., Bressac, M., Dammshäuser, A., Streu, P., Guieu, C., and Croot, P. L.: Impacts of dust
27 deposition on dissolved trace metal concentrations (Mn, Al and Fe) during a mesocosm experiment, *Biogeosciences*, 10,
28 2583-2600, 10.5194/bg-10-2583-2013, 2013.
- 29 Zou, S., Lozier, S., Zenk, W., Bower, A., and Johns, W.: Observed and modeled pathways of the Iceland Scotland
30 Overflow Water in the eastern North Atlantic, *Progress in Oceanography*, 159, 211-222, 10.1016/j.pocean.2017.10.003,
31 2017.
- 32 Zunino, P., Lherminier, P., Mercier, H., Daniault, N., García-Ibáñez, M. I., and Pérez, F. F.: The GEOVIDE cruise
33 in may-June 2014 revealed an intense MOC over a cold and fresh subpolar North Atlantic, *Biogeosciences*, 2017.
- 34
- 35

1 Figure 1: Map of the GEOTRACES GA01 voyage plotted on bathymetry as well as the major topographical features and main
2 basins. Crossover station with GEOTRACES voyage (GA03) is shown as a red star. (Ocean Data View (ODV) software, version
3 4.7.6, R. Schlitzer, <http://odv.awi.de>, 2016). BFZ: Bight Fracture Zone, CGFZ: Charlie-Gibbs Fracture Zone.

4

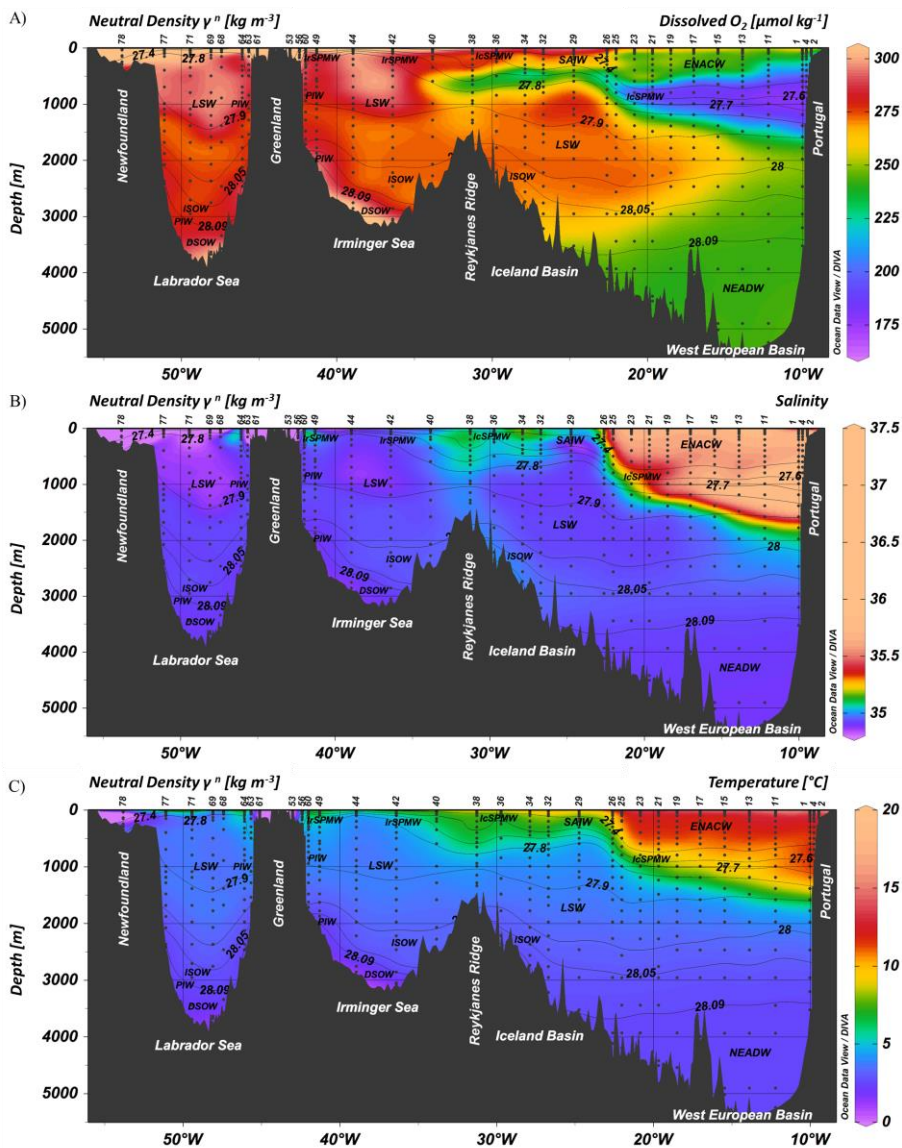
5



6

7

- 1 Figure 2: Parameters measured from the regular CTD cast represented as a function of depth for GA01 section for (A) Dissolved
- 2 Oxygen (O_2 , $\mu\text{mol kg}^{-1}$), (B) Salinity and (C) Temperature ($^{\circ}\text{C}$). The contour lines represent isopycnals (neutral density, γ^n , in units
- 3 of kg m^{-3}).



Surface water masses

ENACW	East North Atlantic Central Water
IcSPMW	Iceland SubPolar Mode Water
IrSPMW	Irminger SubPolar Mode Water
SAIW	Subarctic Intermediate Water

Intermediate water masses

MOW	Mediterranean Outflow Water
LSW	Labrador Sea Water

Overflow Deep water masses

NEADW	North East Atlantic Deep Water
PIW	Polar Intermediate Water
ISOW	Iceland-Scotland Overflow Water
DSOW	Denmark Strait Overflow Water

Figure 3: Contour plot of the distribution of dissolved iron (DFe) concentrations in nmol L^{-1} along the GA01 voyage transect: upper 1000 m (top) and full depth range (bottom). The red dashed line indicates the depth of the Surface Mixed Layer (SML). Small black dots represent collected water samples at each sampling station. (Ocean Data View (ODV) software, version 4.7.6, R. Schlitzer, <http://odv.awi.de>, 2016).

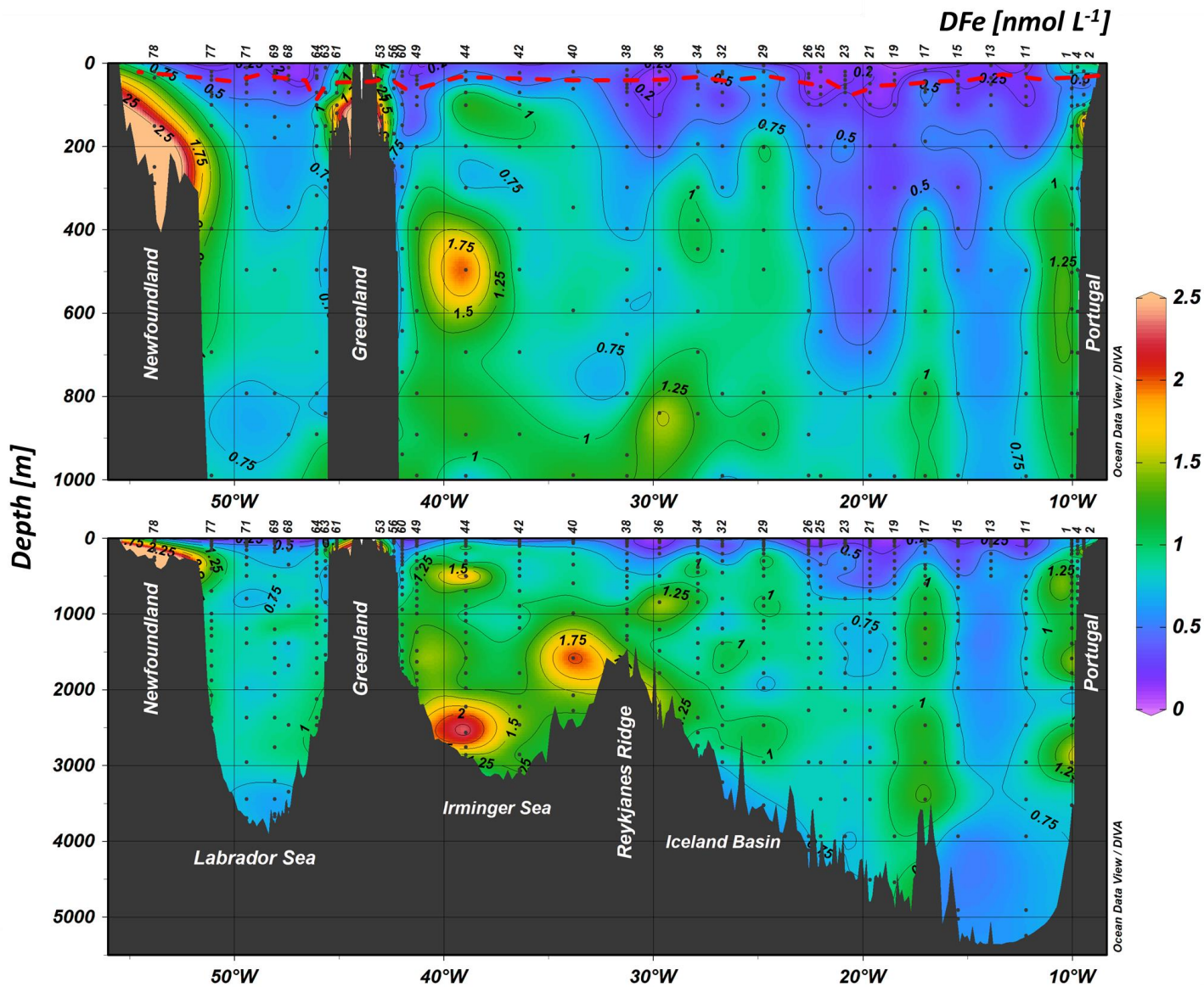


Figure 4: Vertical profiles of dissolved iron (DFe, black dots, solid line), particulate iron (PFe, black open dots, dashed line, Gourain et al., in prep.) and dissolved aluminium (DAI, grey dots, Menzel Barraqueta et al., 2018) at Stations 2 (A), and 4 (B) located above the Iberian shelf, Station 56 (C), Stations 53 (D) 53 and Station 61 (E) located above the Greenland shelf and Station 78 (F) located above the Newfoundland shelf. Note that for stations 53, 61 and 78, plots of the percentage of meteoric water (open dots) and sea-ice (black dots and dashed line) (Benetti et al., see text for details), Total Chlorophyll-*a* (TChl-*a*, green), temperature (blue) and salinity (black) are also displayed as a function of depth.

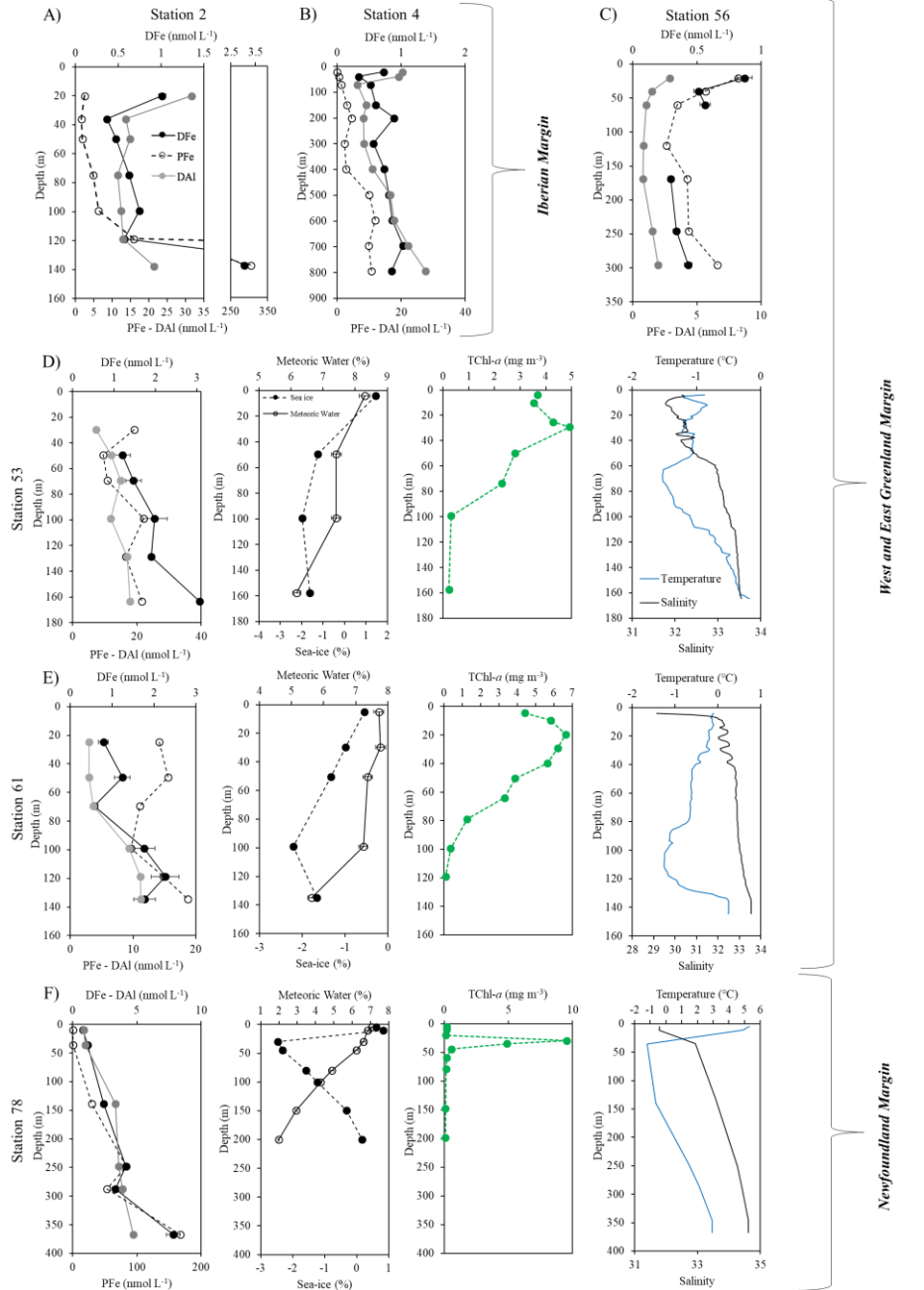


Figure 5: Plot of dissolved iron (DFe, black circles) and dissolved aluminium (DAI, white circles, Menzel Barraqueta et al., 2018) along the salinity gradient between stations 1, 2, 4, 11 and 13 with linear regression equations. Numbers close to sample points representing station numbers.

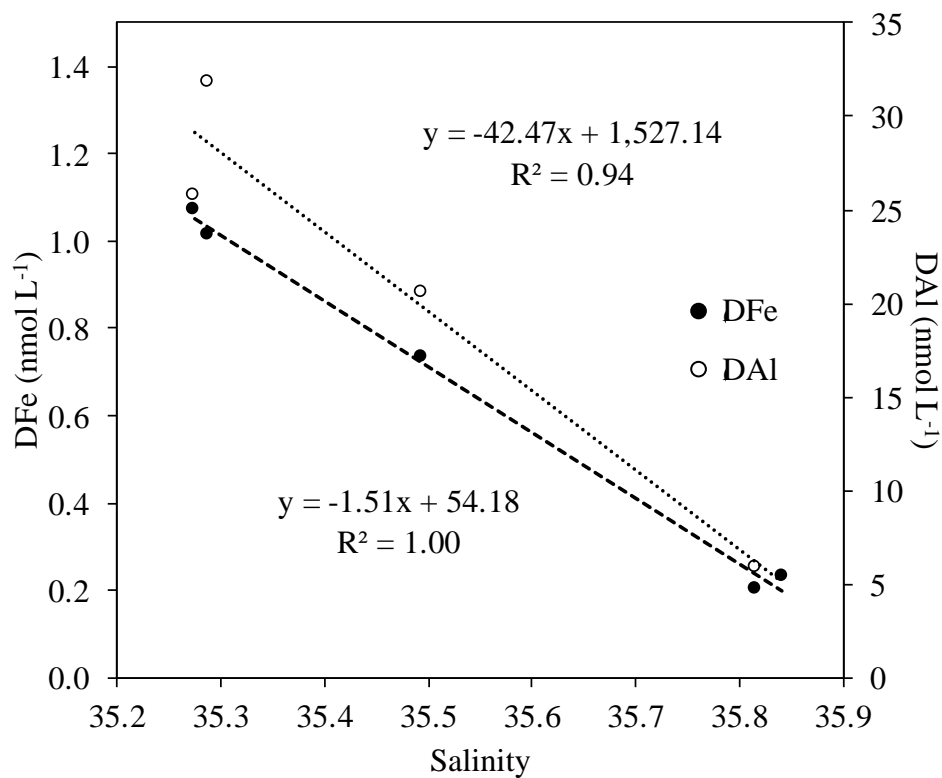


Figure 6: Plot of dissolved Fe (DFe) Turnover Times relative to Atmospheric Deposition (TTADs) calculated from soluble Fe contained in aerosols estimated from a two-stage sequential leach (UHP water, then 25% HAc, Shelley et al., this issue). Note that numbers on top of points represent station numbers and that the colour coding refers to different region with in yellow, margin stations; in purple, the West European Basin; in blue, the Iceland Basin; in green, the Irminger Sea and in red, the Labrador Sea. The numbers on top of the plot represent TTADs averaged for each oceanic basin and their standard deviation.

5

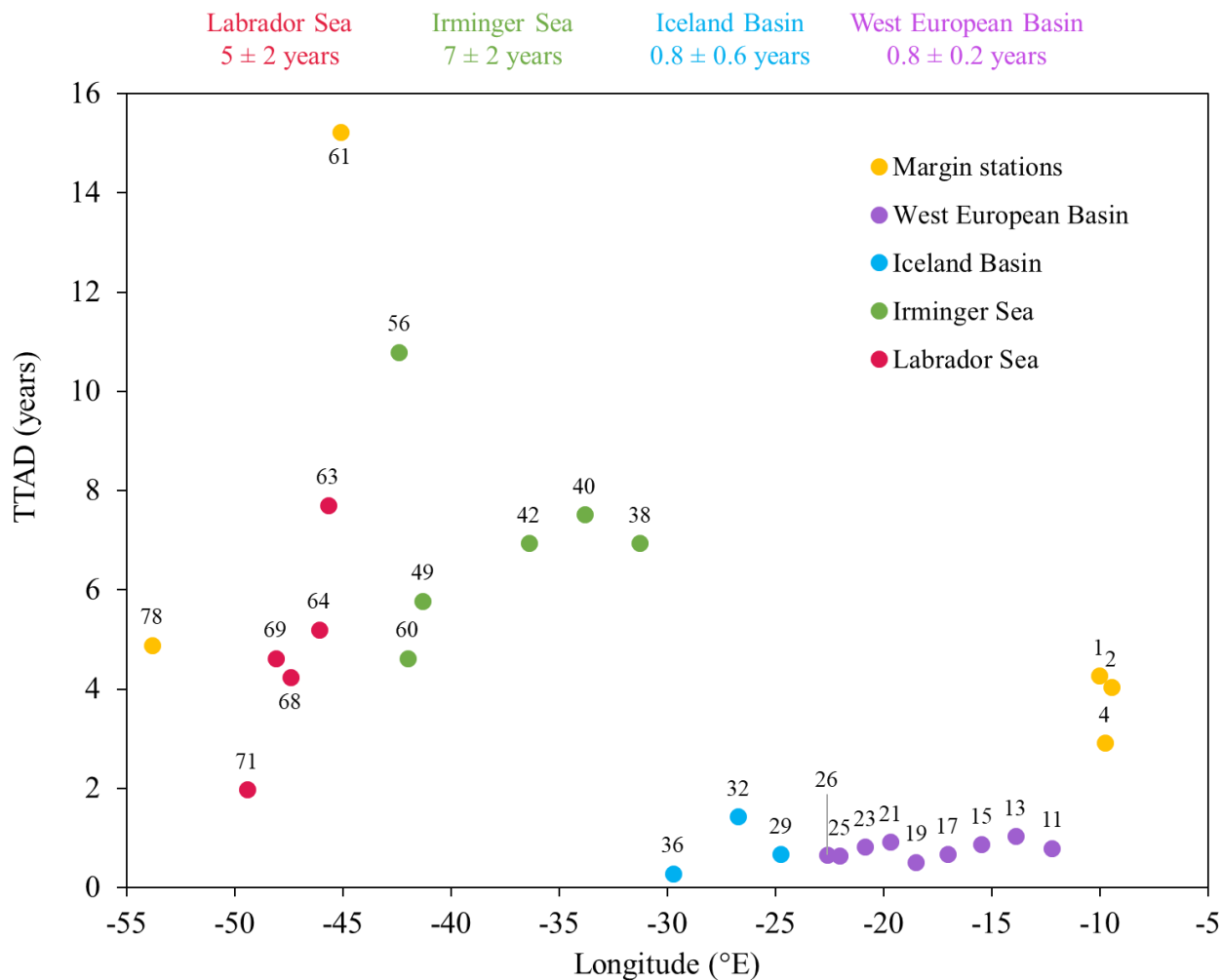
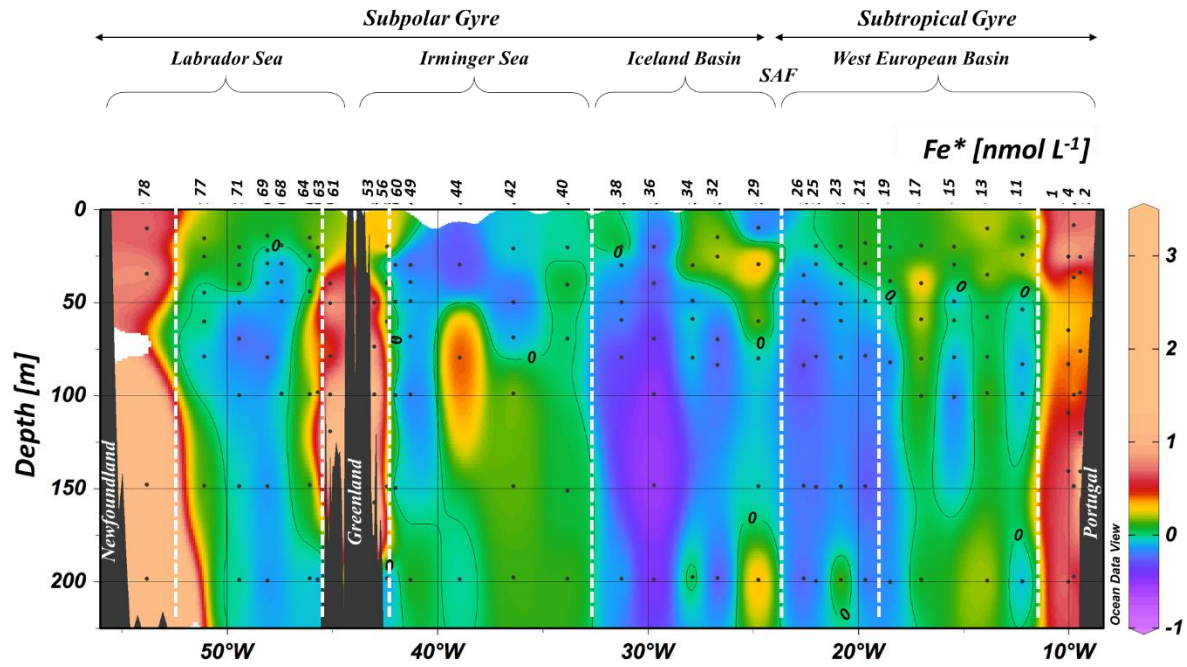


Figure 7: Section plot of the Fe* tracer in the North Atlantic Ocean with a remineralization rate ($R_{Fe:N}$) of $0.05 \text{ mmol mol}^{-1}$ from surface to 225 m depth. A contour line of 0 separates areas of negative Fe* from areas with positive Fe*. Positive values of Fe* imply there is enough iron to support complete consumption of NO_3^- when this water is brought to surface, and negative Fe* values imply a deficit. See text for details.



Station	Date sampling	filtration μm	Latitude $^{\circ}\text{N}$	Longitude $^{\circ}\text{E}$	Z_m m	DFe (nmol L ⁻¹)			
	DD/MM/YYYY					average	SD	n	
1	19/05/2014	0.2	40.33	-10.04	25.8	1.07	±	0.12	1
2	21/05/2014	0.2	40.33	-9.46	22.5	1.01	±	0.04	1
4	21/05/2014	0.2	40.33	-9.77	24.2	0.73	±	0.03	1
11	23/05/2014	0.2	40.33	-12.22	31.3	0.20	±	0.11	2
13	24/05/2014	0.45	41.38	-13.89	18.8	0.23	±	0.02	1
15	28/05/2014	0.2	42.58	-15.46	34.2	0.22	±	0.03	2
17	29/05/2014	0.2	43.78	-17.03	36.2	0.17	±	0.01	1
19*	30/05/2014	0.45	45.05	-18.51	44.0	0.13	±	0.05	2
21	31/05/2014	0.2	46.54	-19.67	47.4	0.23	±	0.08	2
23*	02/06/2014	0.2	48.04	-20.85	69.5	0.21	±	0.05	6
25	03/06/2014	0.2	49.53	-22.02	34.3	0.17	±	0.04	2
26	04/06/2014	0.45	50.28	-22.60	43.8	0.17	±	0.03	2
29	06/06/2014	0.45	53.02	-24.75	23.8	0.17	±	0.02	1
32	07/06/2014	0.2	55.51	-26.71	34.8	0.59	±	0.08	2
34	09/06/2014	0.45	57.00	-27.88	25.6	NA	±		0
36	10/06/2014	0.45	58.21	-29.72	33.0	0.12	±	0.02	1
38	10/06/2014	0.45	58.84	-31.27	34.5	0.36	±	0.16	2
40	12/06/2014	0.45	59.10	-33.83	34.3	0.39	±	0.05	1
42	12/06/2014	0.45	59.36	-36.40	29.6	0.36	±	0.05	1
44	13/06/2014	0.2	59.62	-38.95	25.8	NA	±		0
49	15/06/2014	0.45	59.77	-41.30	60.3	0.30	±	0.05	2
53*	17/06/2014	0.45	59.90	-43.00	36.4	NA	±		0
56*	17/06/2014	0.45	59.82	-42.40	30.0	0.87	±	0.06	1
60*	17/06/2014	0.45	59.80	-42.00	36.6	0.24	±	0.02	2
61*	19/06/2014	0.45	59.75	-45.11	39.8	0.79	±	0.12	1
63*	19/06/2014	0.45	59.43	-45.67	86.7	0.40	±	0.03	1
64	20/06/2014	0.45	59.07	-46.09	33.9	0.27	±	0.06	2
68*	21/06/2014	0.45	56.91	-47.42	26.3	0.22	±	0.01	1
69*	22/06/2014	0.45	55.84	-48.09	17.5	0.24	±	0.02	1
71	24/06/2014	0.45	53.69	-49.43	36.7	0.32	±	0.04	2
77*	26/06/2014	0.45	53.00	-51.10	26.1	NA	±		0
78	27/06/2014	0.45	51.99	-53.82	13.4	0.79	±	0.05	1

5

Table 1: Station number, date of sampling (in the DD/MM/YYYY format), size pore used for filtration (μm), station location, mixed layer depth (m) and associated average dissolved iron (DFe) concentrations, standard deviation and number of samples during the GEOTRACES GA01 transect. Note that the asterisk next to station numbers refers to disturbed temperature and salinity profiles as opposed to uniform profiles.

Seawater used for calibration	SeaFAST-pico™ DFe values (nmol L ⁻¹)			reference or certified DFe values (nmol L ⁻¹)		
	Average	SD	n	Average	SD	
SAFe S	0.100	± 0.006	2	0.095	±	0.008
GSP	0.16	± 0.04	15	NA	±	NA
NASS-7	6.7	± 1.7	12	6.3	±	0.5

Table 2: SAFe S, GSP and NASS-7 dissolved iron concentrations (DFe, nmol L⁻¹) determined by the SeaFAST-pico™ and their consensus (SAFe S, GSP; <https://websites.pmc.ucsc.edu/~kbruland/GeotracesSaFe/kwbGeotracesSaFe.html>) and certified (NASS-7; https://www.nrc-cnrc.gc.ca/eng/solutions/advisory/crm/certificates/nass_7.html) DFe concentrations. Note that yet no consensual value is reported for the GSP seawater.

Margins	Stations #	DFe:DAI (mol:mol)		PFe:PAI (mol:mol)		DFe:PFe (mol:mol)		n
		average	SD	average	SD	average	SD	
<i>Iberian Margin</i>	2 and 4	0.07	± 0.03	0.20	± 0.01	0.13	± 0.09	10
<i>East Greenland Margin</i>	56 and 53	0.21	± 0.09	0.30	± 0.01	0.12	± 0.03	6
<i>West Greenland Margin</i>	61	0.18	± 0.02	0.32	± 0.01	0.14	± 0.04	3
<i>Newfoundland Margin</i>	78	1.1	± 0.41	0.31	± 0.01	0.06	± 0.02	4

Table 3: Averaged DFe:DAI (Menzel Barraqueta et al., 2018) and PFe:PAI (Gourain et al., in prep.) ratios reported per margins. Note that to avoid phytoplankton uptake, only depth below 100 m depth are considered.